rocscience

RS2

Thermal Analysis

Examples

Table of Contents

1. Artificial Ground Freezing in Tunnel Construction

1.1. Problem Description

Artificial ground freezing techniques are often used in construction to reinforce and stabilize soil during excavation. This is achieved by circulating low temperature refrigerants (brine) in freezing pipes which absorbs heat, freezing soils that surround the tunnel. Yan et al (2019) proposed a numerical simulation solution to accurately predict the thickness of the freezing during active freezing of the soil, which is coupled with data collected from field monitoring. This problem will be replicated in RS2 and aims to demonstrate artificial ground freezing modelling and compare RS2 results with that presented by Yan et al.

1.2. Model Geometry

The model domain is 26m wide and a height of 24.7m with a homogeneous sandy clay material. The initial temperature of the domain was set at 25˚C. The top surface of the model was set as a convection surface with a medium temperature of 25˚C and a heat transfer coefficient of 18W/m^2/˚C. The model consists of 46 frozen pipes represented by nodes assigned with a convective heat transfer coefficients of 50 W/m^2/˚C and a medium temperature which reflects the field monitored brine temperatures (Figure 1.2). The perimeter assigned to each node is 0.339 m.

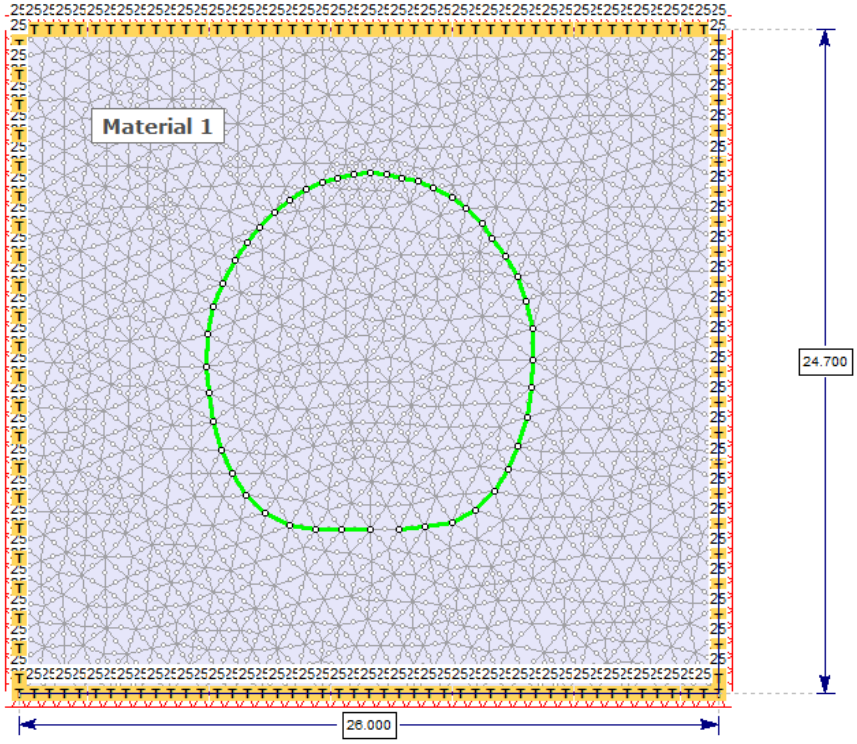

Figure 1.1: RS2 model initial conditions

The simulation runs for the duration of the active freezing period of 130 days (1.1232e+07 secs), the time steps were set to every day and stages set as every 5 days.

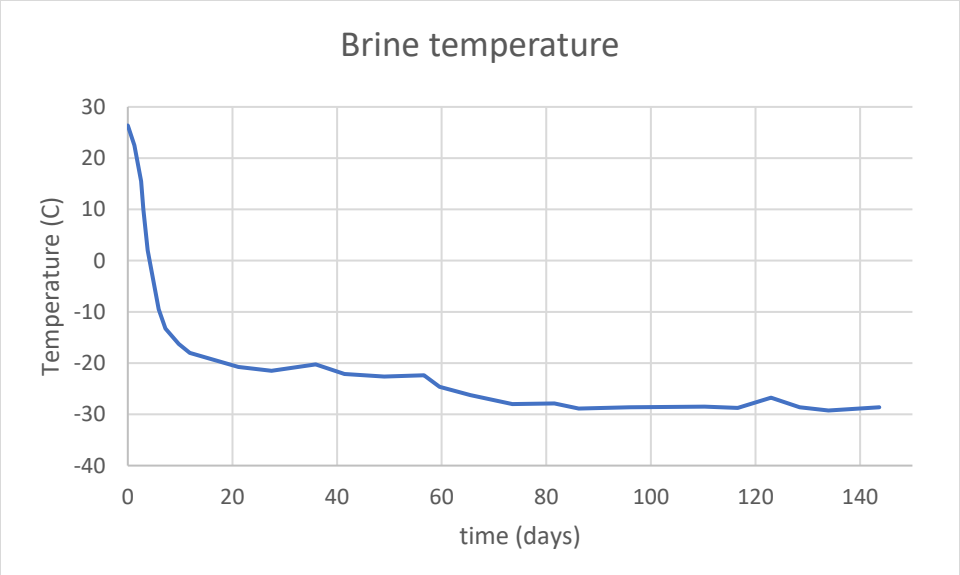

Figure 1.2: Brine (refrigerant) temperature function

1.3. Model parameters

The material properties of the sandy clay can be seen in Table 1.1.

Table 1.1: Material properties

Parameter	Value
Unit weight (kN/m^3)	19.1295
Porosity	0.278
Water content value	0.278
Unfrozen conductivity (W/m/˚C)	1.032
Frozen conductivity (W/m/˚C)	1.393
Frozen temperature (˚C)	-2
Latent heat	Yes
Unfrozen volumetric heat capacity (J/m^3/˚C)	2.09e+06
Frozen volumetric heat capacity (J/m^3/˚C)	2.8e+06
Thermal soil unfrozen water content	Custom
Thermal expansion	No

Table 1.2: Thermal soil unfrozen water content

Temperature	Water content
-2	0
0	0.278

1.4. Results

The extent of the frozen zone ranges from -30 ˚C to -2 ˚C. Figure 1.3 to Figure 1.5 show the temperature profile of the frozen zone from RS2 at day 30, 80 and 130 respectively. The frozen zone is first formed at 30 days from the top with a thickness of 0.7 m, agreeing with the simulation conducted by Yan et al (2019). RS2 results at day 80 and 130 also agree with that of Yan et al (2019). The thickness of the frozen zones increases to 2m at 80 days and 3m at 130 days. The 3m thick frozen zone falls within the theoretical computed thickness from the field monitoring data (Yan et al., 2019) ranging between 2.6m and 4.1 m.

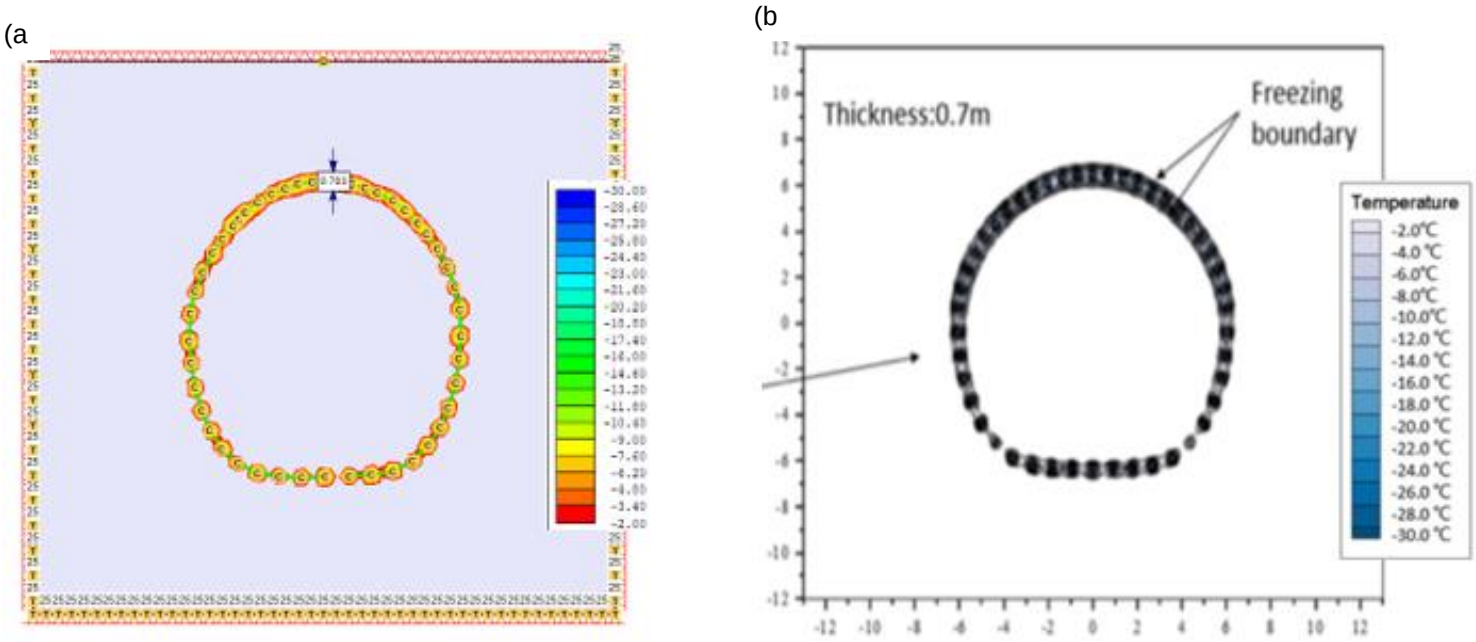

Figure 1.3: Frozen zone at day 30 a) RS2 b) Yan et al., 2019

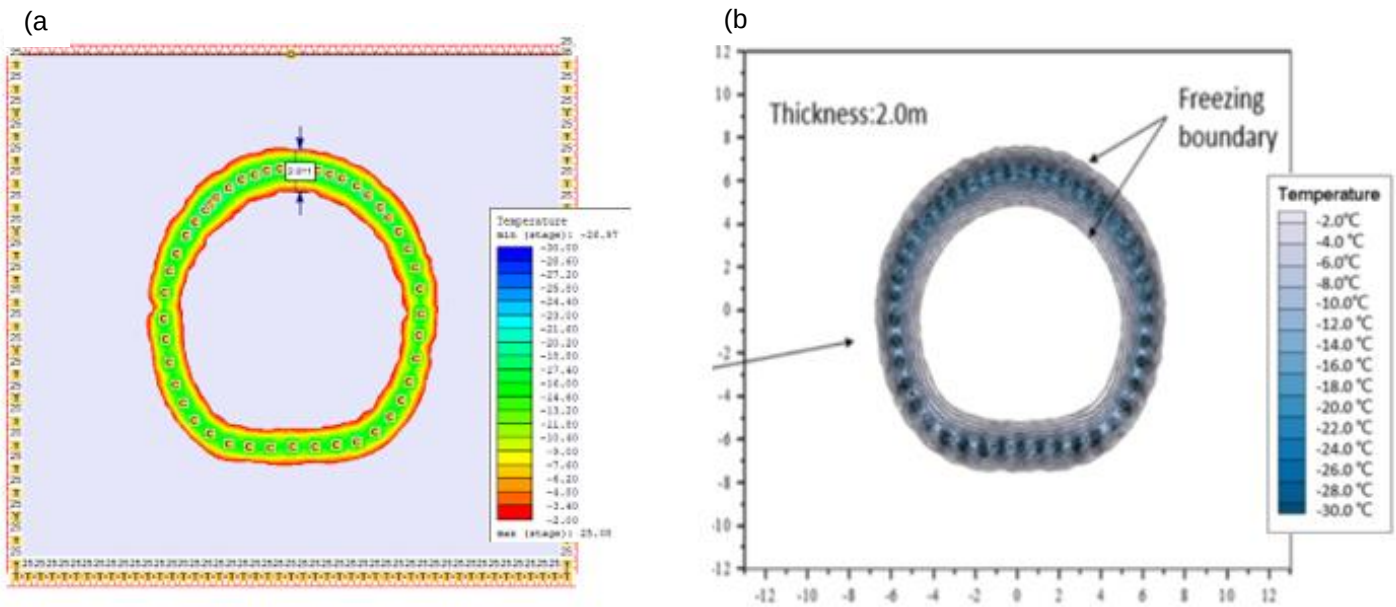

Figure 1.4: Frozen zone at day 80 a) RS2 b) Yan et al., 2019

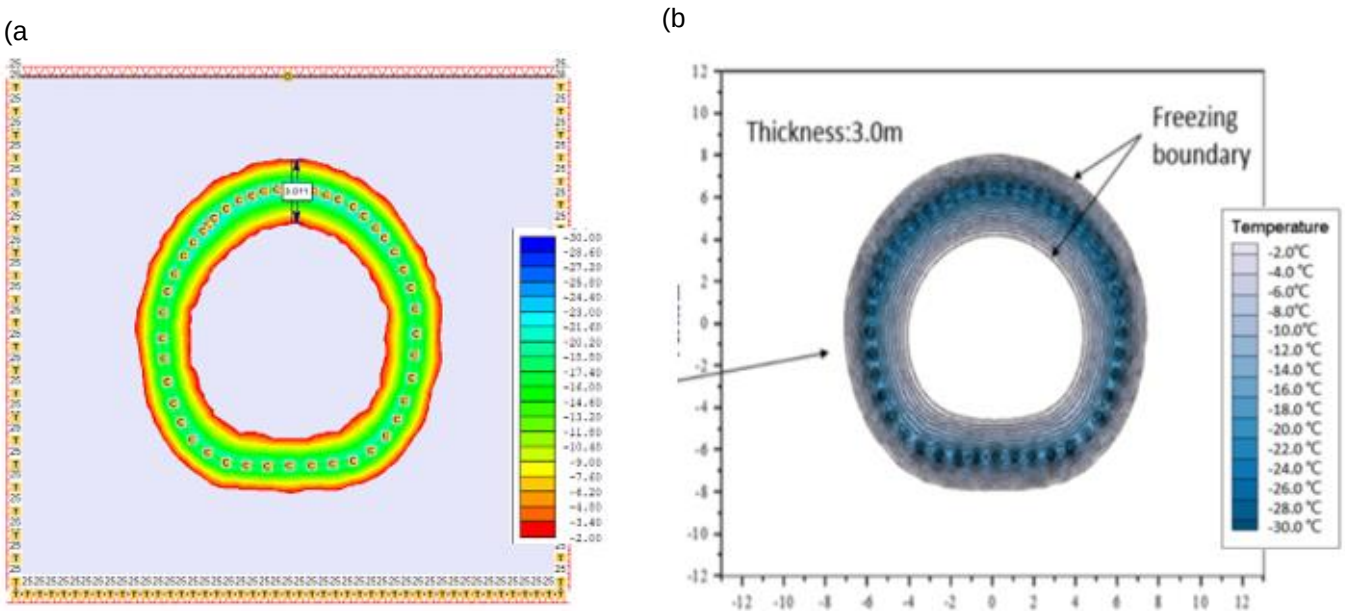

Figure 1.5: Frozen zone at day 130 a) RS2 b) Yan et al., 2019

1.5. References

Yan, Q., Wu, W., Zhang, C., Ma, S. and Li, Y. (2019). Monitoring and Evaluation of Artificial Ground Freezing in Metro Tunnel Construction-A Case Study. *KSCE Journal of Civil Engineering*, 23(5), pp.2359-2370.

2. Convection Embankment

2.1. Problem description

In cold regions the thermal regime of underlying permafrost can be disturbed due to the construction of transport embankments. The use of duct ventilation along embankments was found to prevent or slow down the degradation of the thermal regime in permafrost. The objective of this example is to compare the thermal response of a duct-ventilated embankment, with temperature-controlled shutters to that of a conventional embankment in RS2. The analysis is taken over a four-year period.

2.2. Model geometry

The roadway embankment is 2.5m high and 18m wide with 2:1 side slope. Using symmetry only half the embankment is modelled in each case. The embankment modelled is underlain by a 9m deep, 17m wide silty foundation. An air temperature function representative of the annual conditions in Fairbanks Alaska is applied to the top surface of the domain and a geothermal heat flux of 6e-05 kJ/s/m^2 is kept constant at the bottom of the model. The circular ducts with a perimeter of 0.2m placed at a spacing of 2m will be simulated using a convection surface. This surface is place 0.5m above the foundation layer. The convection surface will simulate the opening and closing of the shutters when the air temperature is above 0˚C. The conventional embankment model will have the same geometry excluding the convectional surface. The geometry of the models is presented in Figure 2.1.

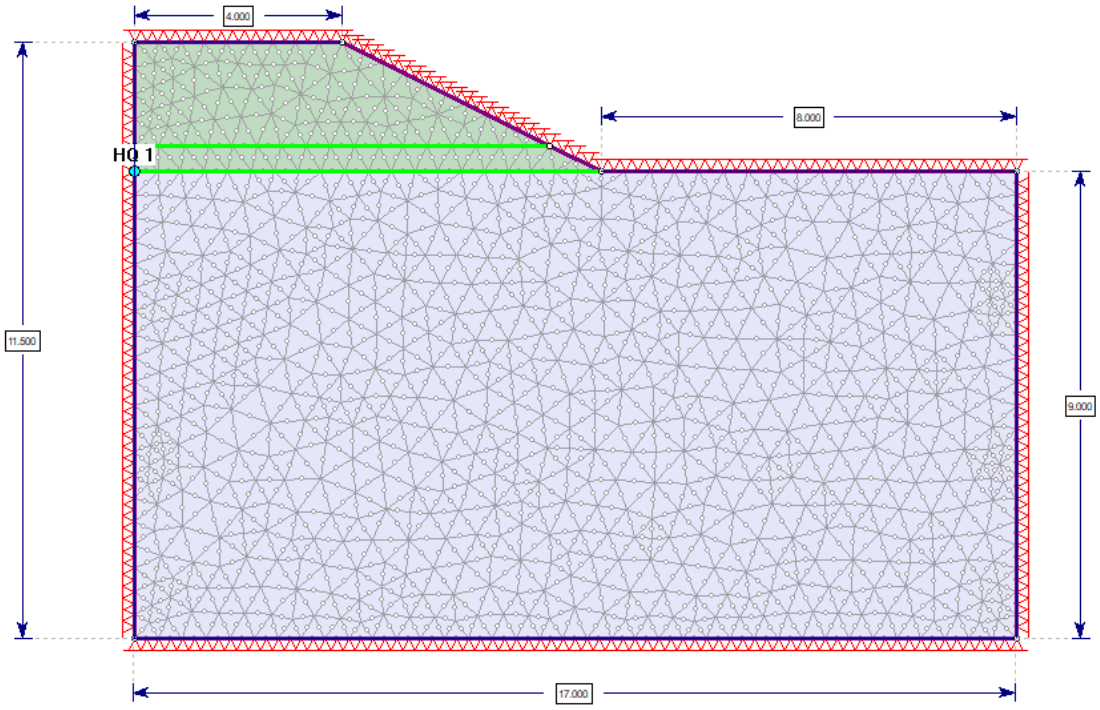

Figure 2.1: RS2 model geometry

2.3. Model properties

The embankment is filled with a relatively dry sand/ gravel mixture. The foundation consists of an ice-rich silt. The thermal properties of each can be found in Table 2.1.

Table 2.1: Material thermal properties

Parameter	Embankment Fill (sand)	Foundation (silt)
Porosity value	0.1	0.649
Water content value (m3/m3)	0.1	0.649
Thermal conductivity method	Constant	Constant
Unfrozen conductivity (kW/m/C)	0.00199	0.00149
Frozen conductivity (kW/m/C)	0.00215	0.00232
Thermal heat capacity method	Constant	Constant
Latent heat	Yes	Yes
Unfrozen volumetric heat capacity (kJ/m^3/C)	1990	3740
Frozen volumetric heat capacity (kJ/m^3/C)	1620	2380
Thermal soil unfrozen water content	Custom	Custom
Thermal expansion	No	No
Dispersivity	No	No

Figure 2.2 and Figure 2.3. show the volumetric unfrozen water content function of each material. Figure 2.4 represents the annual air condition function.

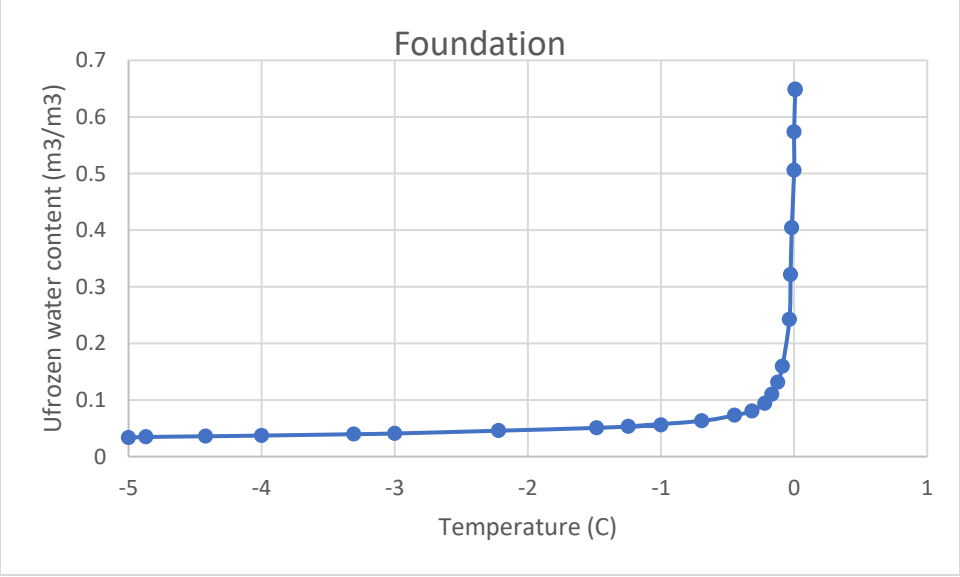

Figure 2.2: Foundation material unfrozen water content function

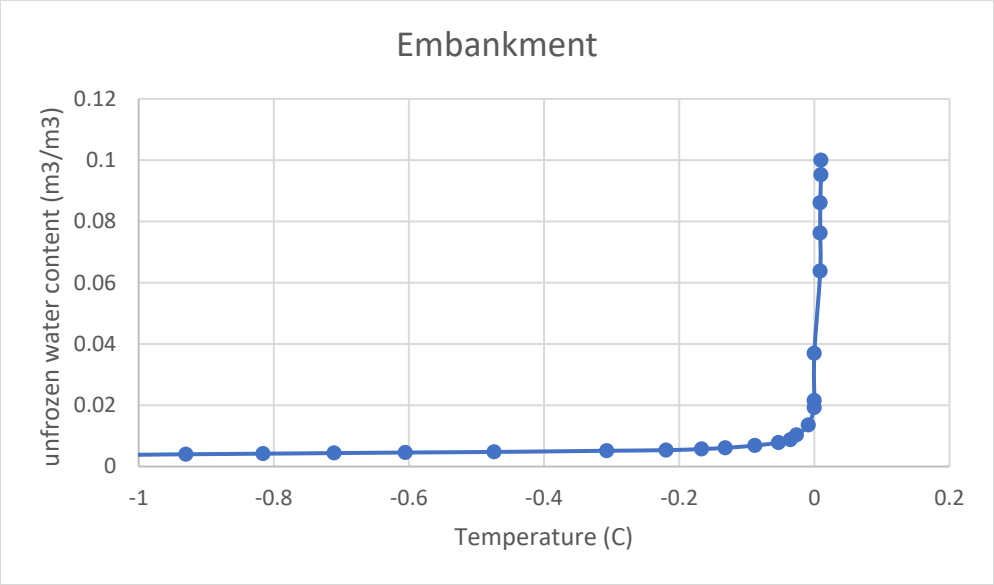

Figure 2.3: Embankment material unfrozen water content function

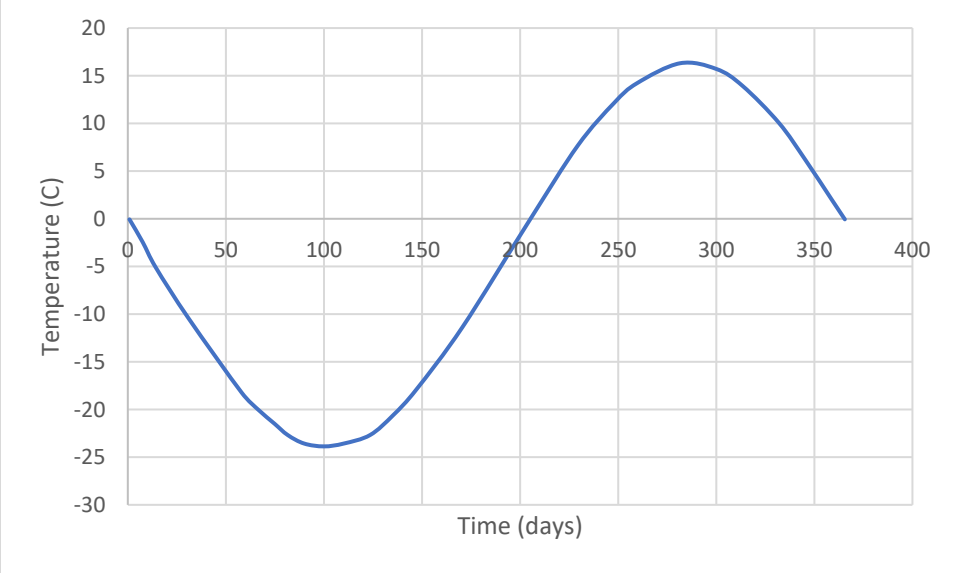

Figure 2.4: Air temperature function (Goering and Kumar, 1996)

2.4. Results

Figure 2.5 shows the temperature at the centre of the embankment/ foundation interface on August 1st of each year over the four-year simulation period. Note the temperature of the embankment without the convection surface has greater temperatures than the embankment with a convection surface.

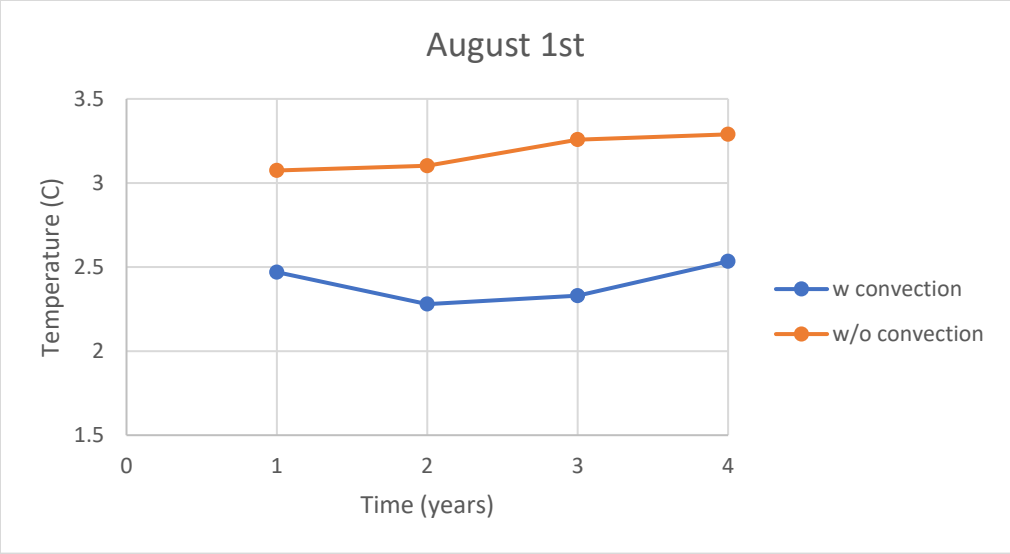

Figure 2.5: Temperature at the centre of the embankment/ foundation interface on August 1st each year

Figure 2.6 shows the temperature profile along the centreline during the last year of simulation. The embankment with convection has lower average temperature than the embankment without convection.

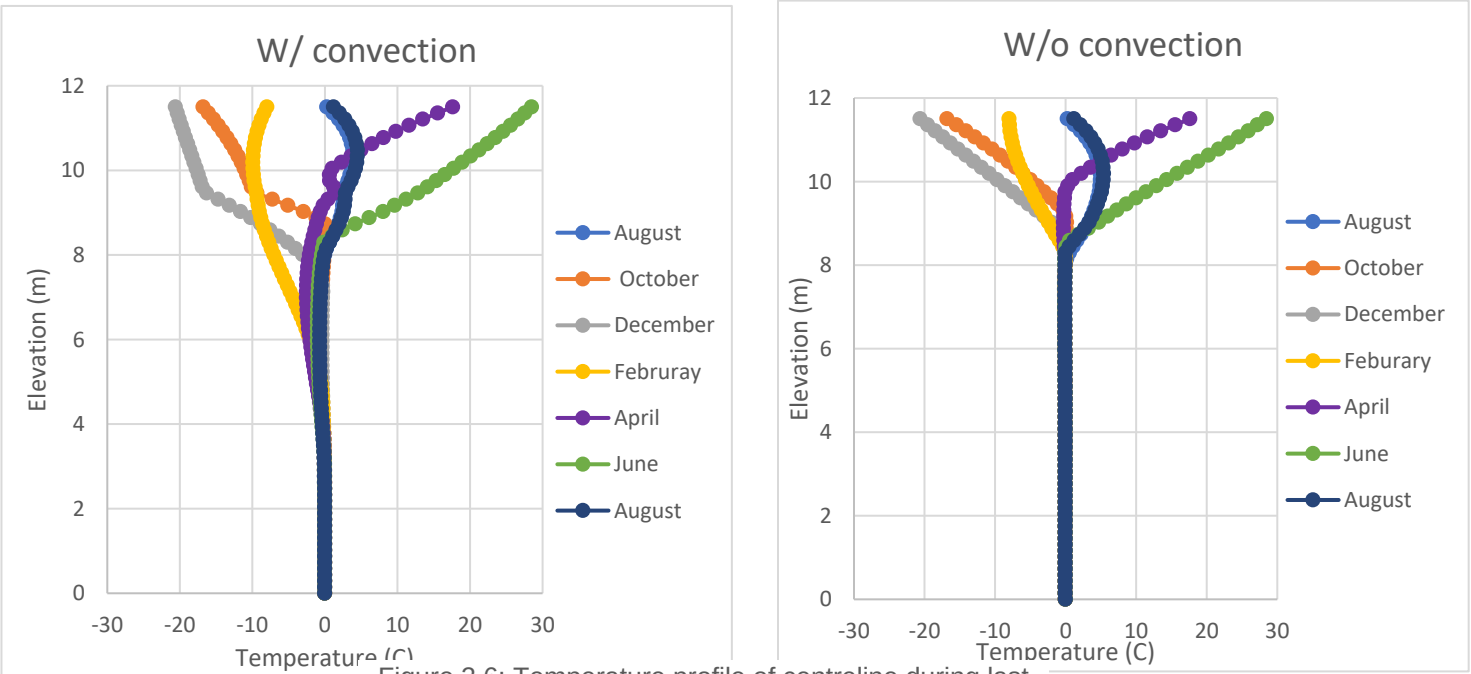

Figure 2.6: Temperature profile of centreline during last year of simulation

2.5. References

Goering, D., & Kumar, P. (1996). Winter-time convection in open-graded embankments. *Cold Regions Science And Technology*, *24*(1), 57-74. doi: 10.1016/0165-232x(95)00011-y.

3. Effect of flowing water on freezing around a pipe

3.1. Introduction

This example focuses on the effect groundwater flow can have on ground freezing around a freeze pipe. Heat flow via forced convection induced by water transfer is often more effective at moving energy than conduction alone. However, the development of pore-ice during ground freezing also impedes groundwater flow due to pore blockage. Three analyzes will be conducted to observe the effect of each factor mentioned.

3.2. Background

Researchers have found a strong similarity between the soil water curve (the relationship between pore water suction and moisture content) and the soil freezing curve (the relationship between sub zero temperatures and the unfrozen water content) of which most models use to be able to predict the unfrozen water content in freezing soils (Kurylyk and Watanabe, 2013). During freezing, the soil would experience the same drop in water content and pore-water pressure as during soil drying. The suction of frozen soil is also equal to the suction in unfrozen soil at the same water content.

There is a non-linear change in suction in frozen soils from 0 to -1 ˚C. Assuming an equivalent change in pressure within water and ice, the equilibrium relationship between temperature and pressure in freezing soils given by the Clausius-Clapeyron equation can determine the change in the freezing point of water:

$$\frac{\partial u_w}{\partial T} = \frac{\partial u_{ice}}{\partial T} = \frac{h_{sf}}{(v_w - v_{ice})T_0} \quad (3.1)$$

Where u_w and u_{ice} are pore-pressures for water and ice, respectively, h_{sf} is latent heat of fusion, v_w and v_{ice} are the specific volumes of water and ice, respectively, and T_0 is the normal freezing point of water at atmospheric pressure. In drying soils there is a discontinuity between ice pressure and water pressure. Assuming that the ice pressure remains at atmospheric pressure, a simplified form of equation (3.1) can be derived:

$$\frac{\partial u_w}{\partial T} = \frac{h_{sf}}{v_w T_0} \quad (3.2)$$

Equation (3.2) indicates a decrease in water pressure per degree Celsius which is considered to emulate the results of laboratory experiments and is used to determine frozen soil matric suction. The suction is then used to determine the hydraulic conductivity from the hydraulic conductivity function.

3.3. Model Geometry

The model is 3 m wide and 1.6 m in height and comprises a circular pipe in the middle at (1.5, 0.8) with a radius of 0.15 m, as seen in Figure 3.1. The temperature of the top and bottom boundary is 3 ˚C and 3.1 ˚C, respectively. The pipe thermal boundary condition is set to a temperature versus time function such that the pipe cools from 3 ˚C to -2 ˚C over a period of 1 day (Figure 3.2). The temperature remains constant at -2 ˚C onward. The hydraulic boundary conditions were selected to establish a lateral groundwater flux. The left boundary is set to 2m head condition and right boundary to 2.1m head condition.

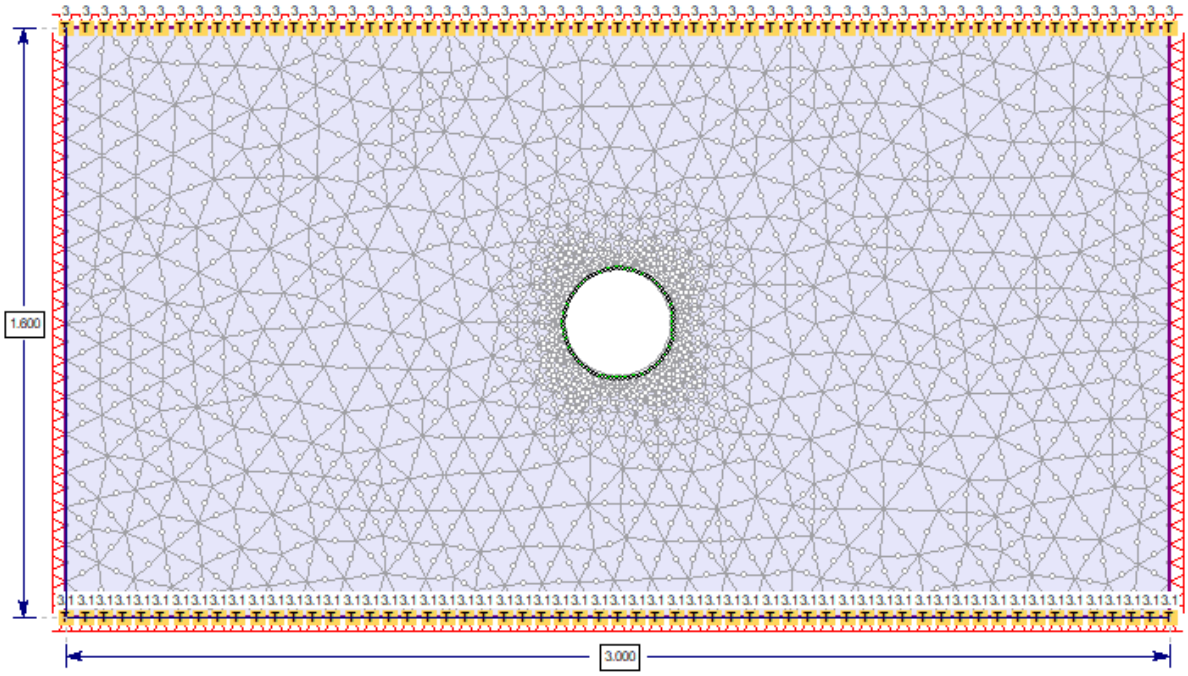

Figure 3.1: Model geometry

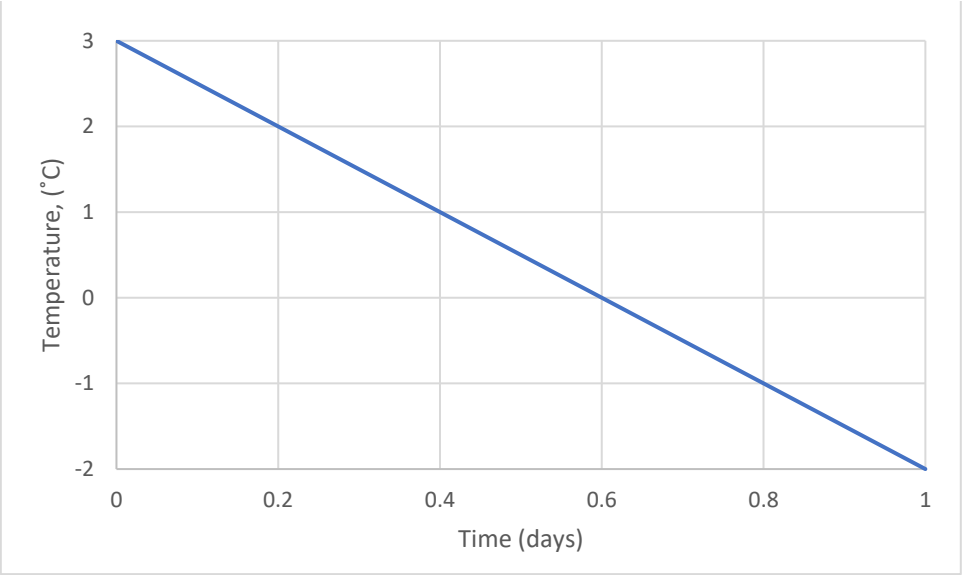

Figure 3.2: Temperature vs. time boundary function over day 1 for pipe cooling

The analysis is taken over the period of 730 days (6.3072e+07 s).

3.4. Model properties

Three transient analyses were conducted. The thermal project setting of each analysis is seen in Table 3.1 and material properties used in each analysis is shown in Table 3.2.

Table 3.1: Thermal project settings

Analysis Type	Forced convection	Pore-ice induced seepage
Conduction only	off	off
Forced Convection	on	off
Forced convection and Pore-ice blockage	on	on

Table 3.2: Material properties

Parameters	Value
Hydraulic properties	
Model	Van Genuchten
Material behaviour	Drained
Ks (m/s)	1e-04
K2/K1	1
K1 angle (degrees)	0
WC sat (m^3/m^3)	1e-05
WC res (m^3/m^3)	0
Mv (m3/m3/kPa)	1e-05
Alpha (1/m)	14.5
N	2.68
Custom m	No
Thermal Properties	
Water content (m3/m3)	0.3
Thermal Conductivity method	Custom
Dependency	Temperature

Thermal volumetric heat capacity type	Constant
Include latent heat	Yes
Unfrozen heat capacity (kJ/m^3/˚C)	2100
Frozen heat capacity (kJ/m^3/˚C)	2100
Frozen temperature (˚C)	0
Thermal soil unfrozen water content type	Custom

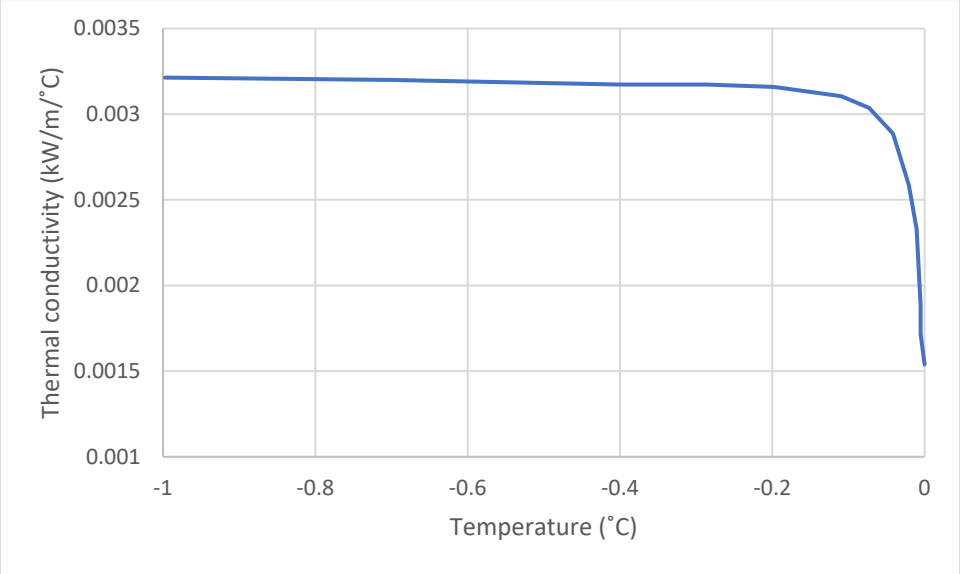

Figure 3.3: Thermal conductivity function

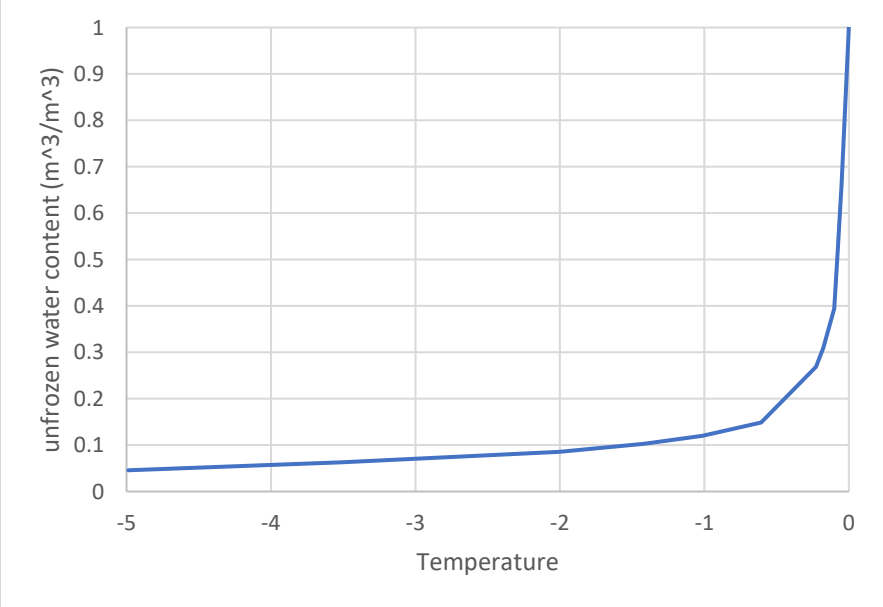

Figure 3.4: Unfrozen water content function

3.5. Results

Figure 3.5 shows the temperature contours and freezing front location of the conduction- only analysis after 2 years. The freezing front has propagated outward from the pipe in an oblong shape.

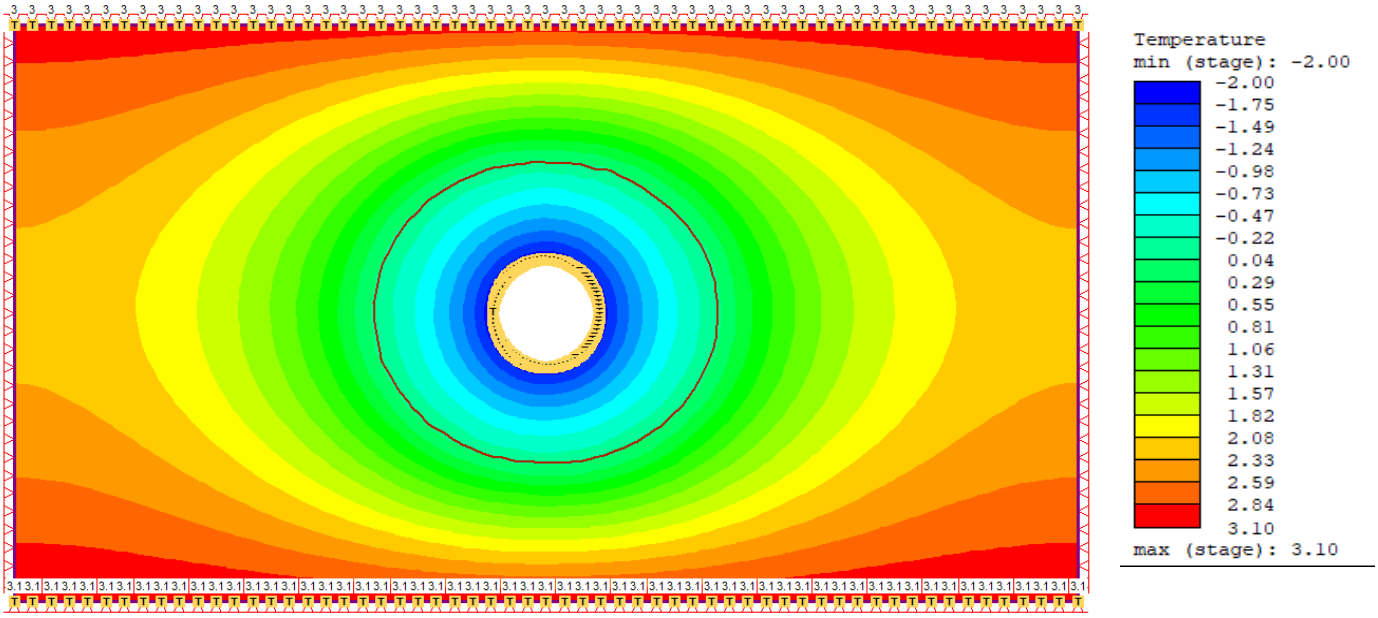

Figure 3.5: Temperature contours and freezing front location for conduction-only analysis

Figure 3.6 shows the results of the forced convection analysis after 2 years. The flow of heat from right to left via convection due to the flowing water has mitigated the propagation of the freezing front in the upstream direction and extended its location in the downstream compared to the conduction-only analysis. Figure 3.7 shows the results of the forced convection and pore-ice blockage analysis. The water flow is clearly impeded within the frozen zone, demonstrating the effects of impeding water flow due to pore-ice blockage. It should be noted that the propagation of the freezing front in the downstream direction has not expanded much further than in the conduction-only analysis. This occurs due to the relatively stagnant water flow withing the freezing front, which implies conduction is the dominant transport mechanism.

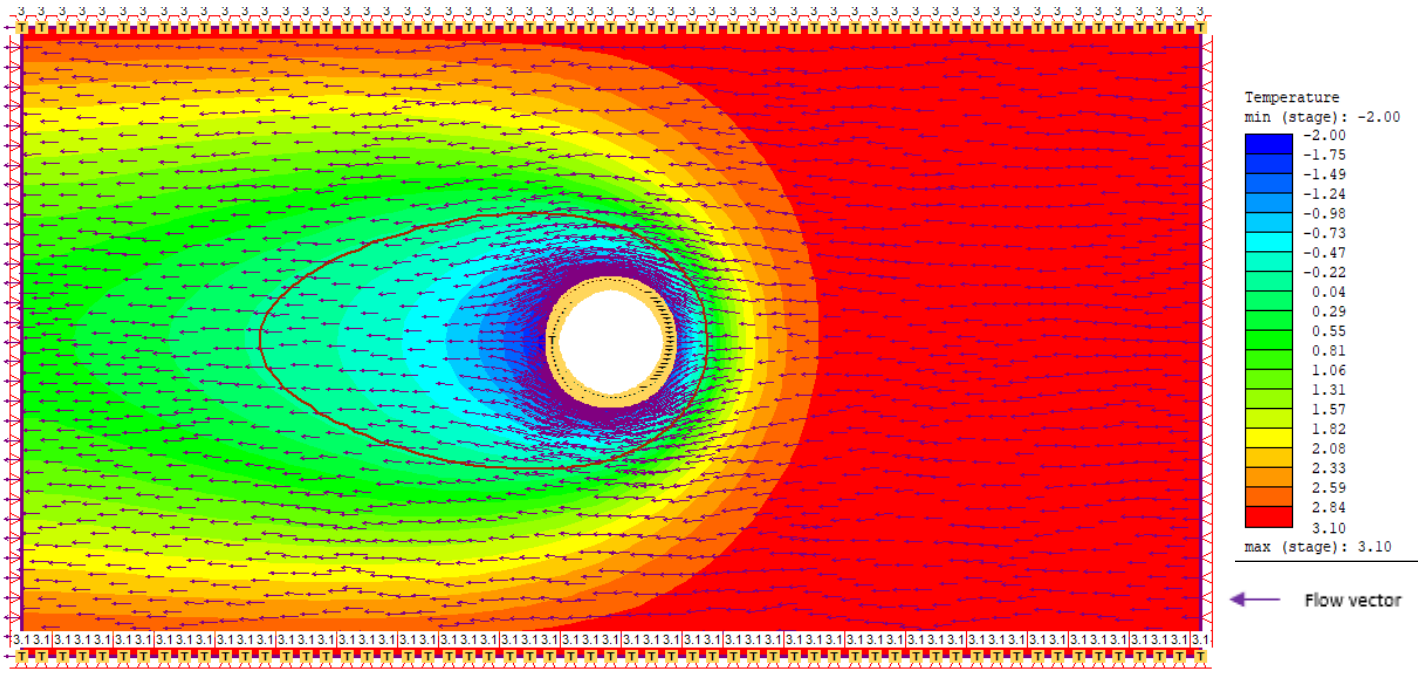

Figure 3.6: Temperature contours, freezing front location and flow vectors for the forced convection analysis

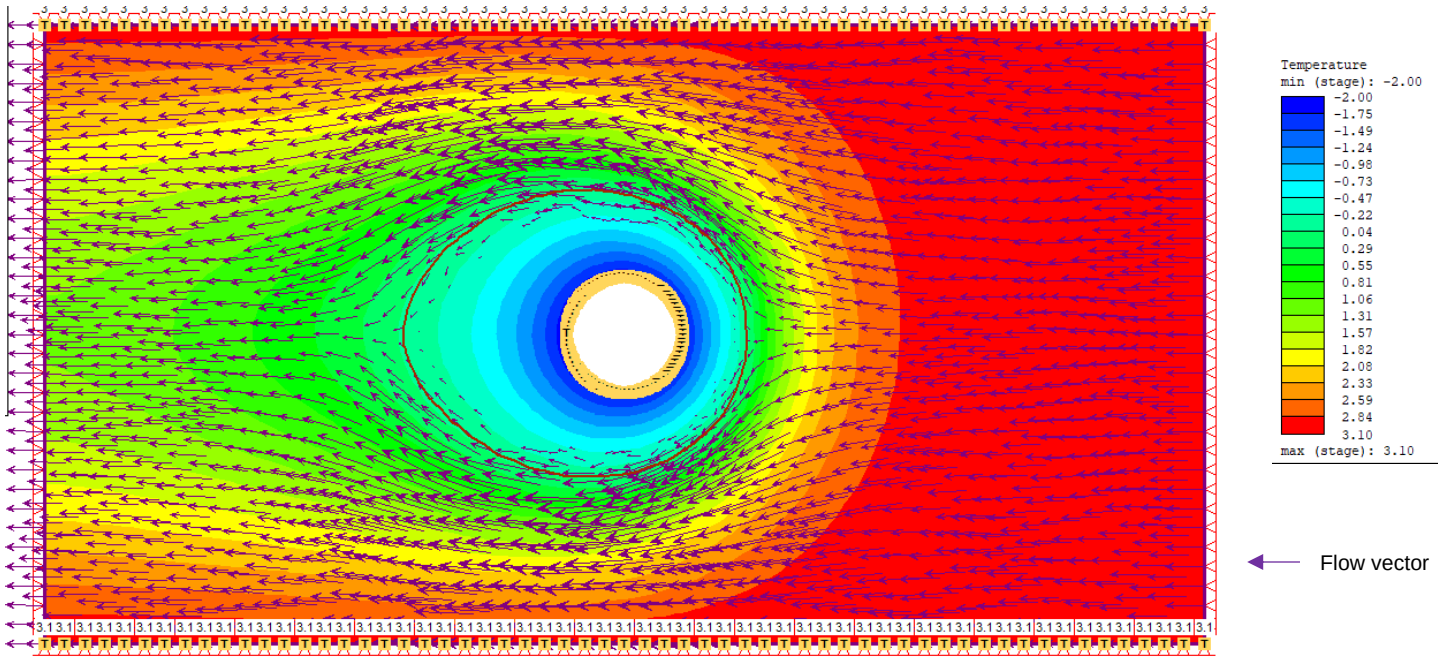

Figure 3.7: Temperature contours, freezing front location vectors for the forced convection and pore-ice blockage analysis

3.6. References

Flerchinger, G.N., Seyfried, M.S., and Hardegree, S.P. (2006). Using soil freezing characteristics to model multi-season soil water dynamics. *Vadose Zone Journal, 5, pp.1143-1153.*

Kurylyk, B. and Watanabe, K. (2013). The mathematical representation of freezing and thawing processes in variably-saturated, non-deformable soils. *Advances in Water Resources, 60, pp.160-177.*

Schofield, R. K. (1935). The pF of the water in soil. *Third International Congress on Soil Science, 2, pp.37-48, 3, pp.182-186.*

Spaans, J.A., and Baker, J.M. (1996). The soil freezing characteristic: its measurement and similarity to the soil moisture characteristic. *Soil Science Society of America Journal, 60, pp. 13 -19.*

4. Frozen Containment Wall

4.1. Problem Description

In this example the RS2 model simulates a hypothetical freezing wall intersecting warm porewater flowing into a domain. The results will be compared to the simulation conducted by McKenzie, Voss & Siegel (2007). The analysis taken over a period of 800 days until steady state is reached.

4.2. Model Geometry

The domain has a width of 50m and height 10m with an initially temperature of 5˚C. The freezing wall has the coordinates (20,0), (20.5,0), (20.5,5) and (20,5) and boundaries are set to a temperature of -5˚C. The left boundary and right boundary of the domain pore pressures are set as 0.5 kPa and 0 kPa, respectively. This creates a ground flow from left to right boundary. The left boundary is kept at 5˚C so the water recharging the domain has a temperature of 5˚C. Note that the forced convection and pore ice seepage options are activated in thermal project settings.

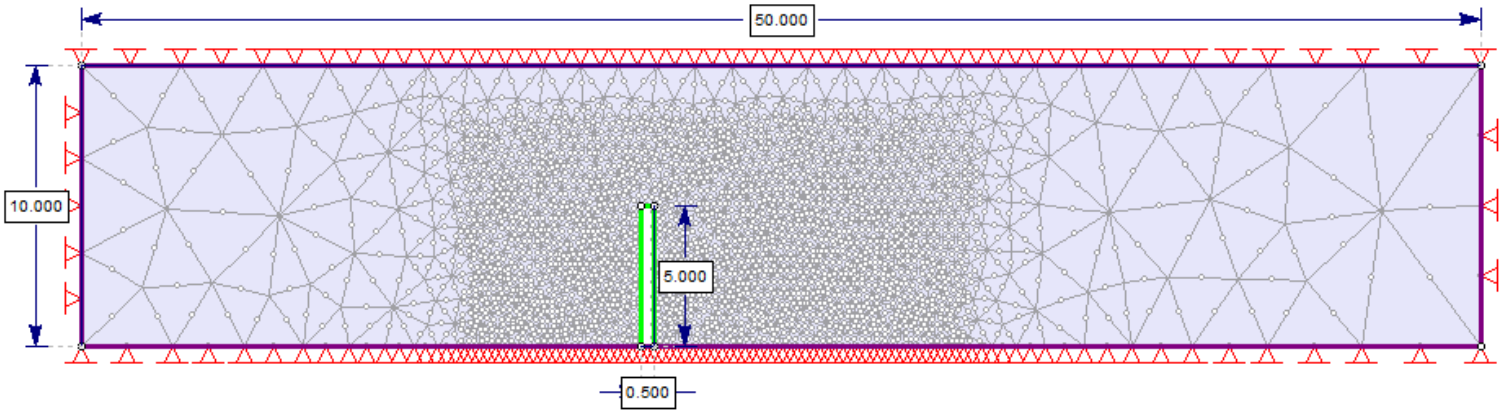

Figure 4.1: RS2 Model geometry

4.3. Material Properties

The material properties of the sand material surround the frozen wall is described in Table 4.1, user define permeability and water content presented in Figure 4.2 and Figure 4.3, respectively, and unfrozen water content function presented in Figure 4.4.

Table 4.1: Material properties

Parameter	Value
Porosity value	0.1
Hydraulic properties	
Model type	User defined
Material behavior	Drained

K2/K1	1
K1 angle (Degrees)	0
Use mv	Yes
Thermal properties	
Water content (m3/m3)	0.1
Thermal conductivity method	Constant
Unfrozen conductivity (kW/m/C)	0.00336
Frozen conductivity(kW/m/C)	0.00321
Thermal heat capacity method	Jame Newman
Latent heat	Yes
Soil heat capacity (kJ/tons/C	840
Thermal soil unfrozen water content	custom
Thermal expansion	No
Dispersity	yes
Longitudinal dispersivity (m)	5
Transverse dispersivity (m)	0.5

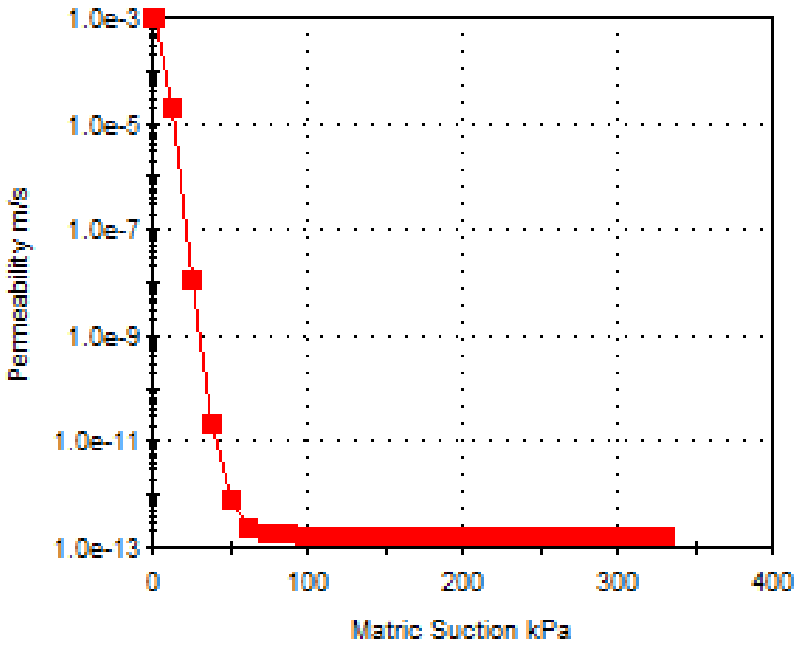

Figure 4.2: User defined permeability function

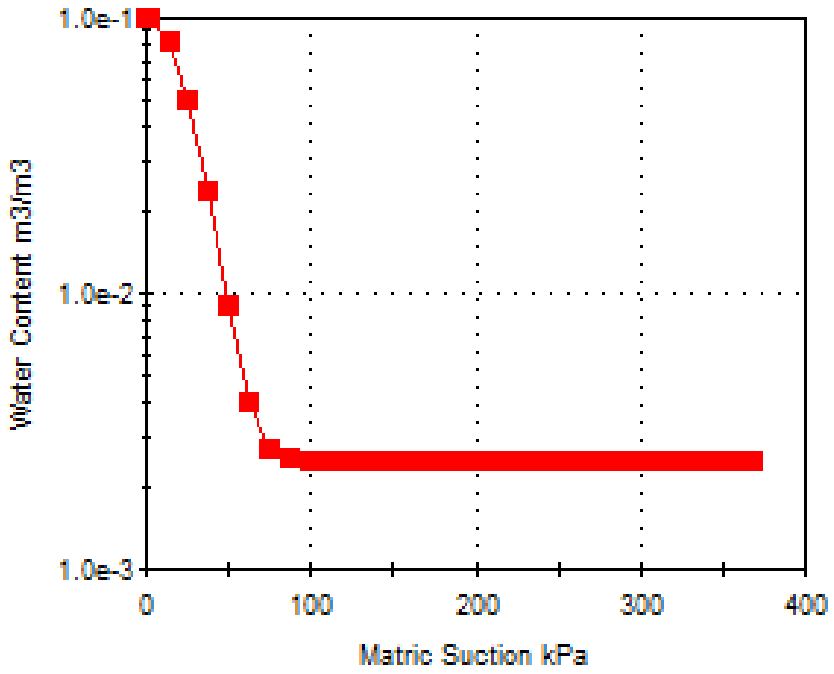

Figure 4.3: User defined water content

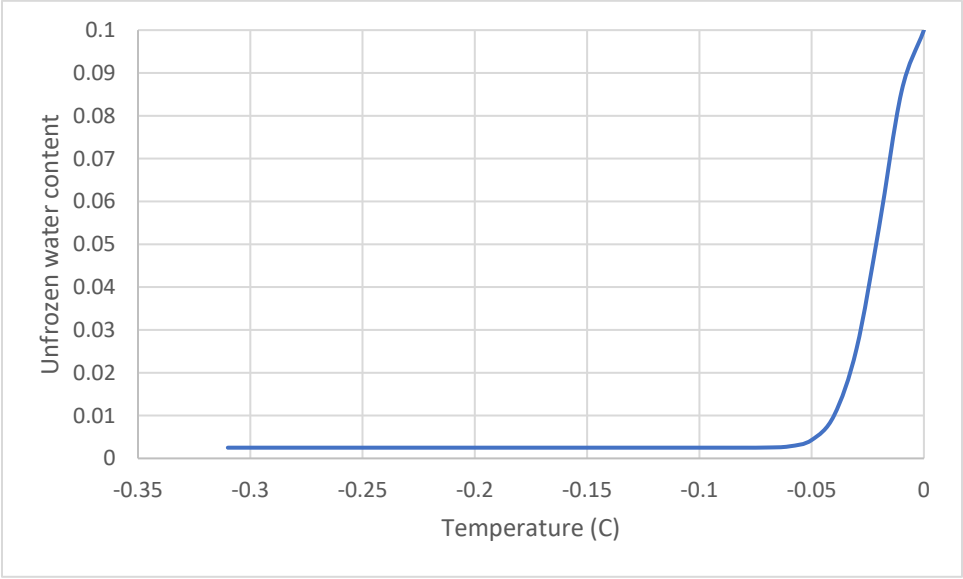

Figure 4.4: Unfrozen water content function

4.4. Results

Figure 4.5 compares the temperature contour at 800 days (steady state) of the RS2 simulation and results provided by McKenzie, Voss & Siegel (2007). Figure 4.6 shows the RS2 flow vectors. It should be noted that velocity is increased around the ice wall. The ice wall forces the pore water to flow around it at higher velocity due to decreases flow area, which agrees with the simulation conducted by McKenzie, Voss & Siegel (2007).

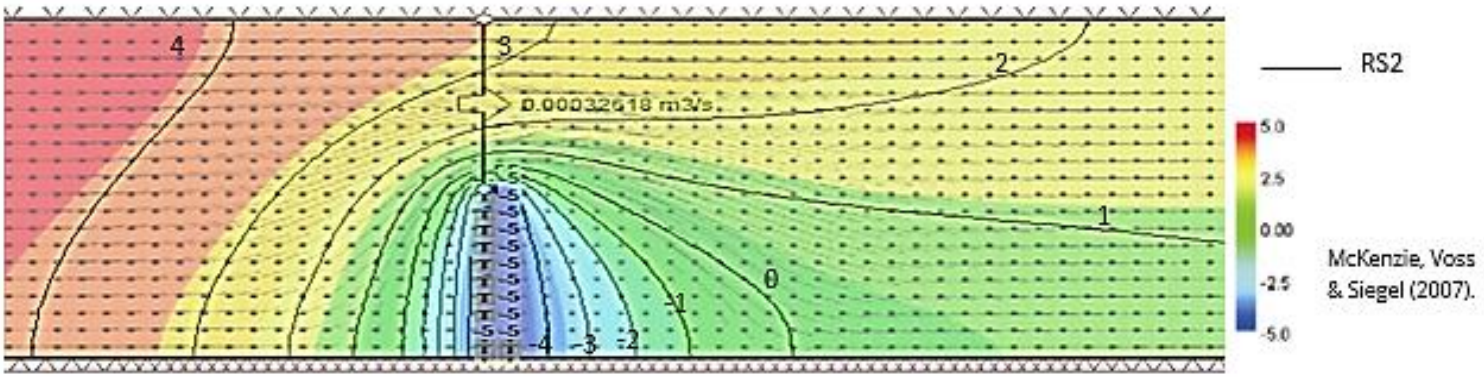

Figure 4.5: Temperature contours at steady state (800 days)

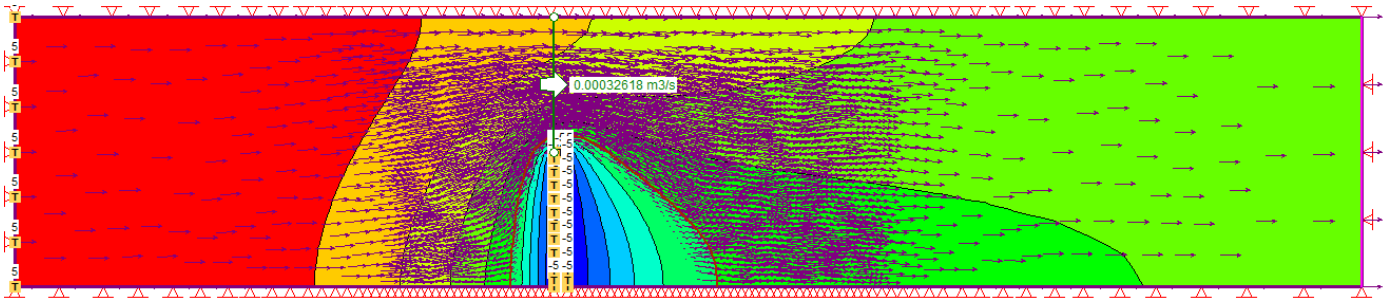

Figure 4.6: RS2 flow vectors at steady state (800) days

4.5. Reference

McKenzie, J., Voss, C., and Siegel, D. (2007). Groundwater flow with energy transport and water–ice phase change: Numerical simulations, benchmarks, and application to freezing in peat bogs. *Advances In Water Resources*, *30*(4), 966-983. *doi: 10.1016/j.advwatres.2006.08.008.*

5. Hill Slope with Seasonal Freezing

5.1. Problem Description

This problem illustrates a simplified cold region water flow system, wherein recharge from a local topographic high discharge to two lakes with different surface elevations. The example is taken from McKenzie, Voss & Siegel (2007) and will demonstrate RS2 ability to simulate the annual water flow system as it changes.

5.2. Model Geometry

The geometry of the slope is specified in Figure 5.1 through Figure 5.4. It should be noted that the exchange of energy between the atmosphere and the ground surface is represented by using a boundary layer 1m thick. The air temperature is applied at the top of this surface and described by a sinusoidal function (Figure 5.5). The left and right lake bottom are assigned a total head of 25m and 21m, respectively. The boundary right below the air and ground interface layer is assigned as a zero-pressure boundary to represent land surface. The initial temperature of the domain is 2˚C. The lake bottom boundaries are kept this constant temperature (2˚C) throughout the analysis.

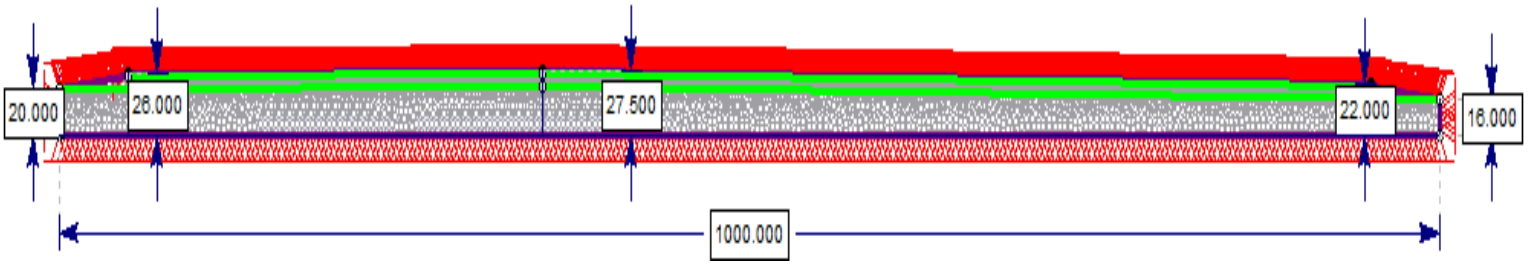

Figure 5.1: RS2 entire model geometry

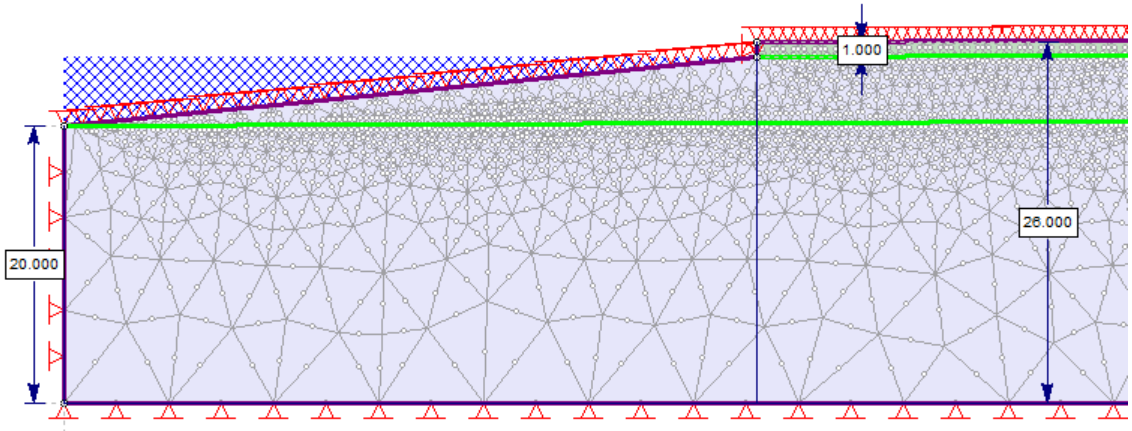

Figure 5.2: Left side of model geometry

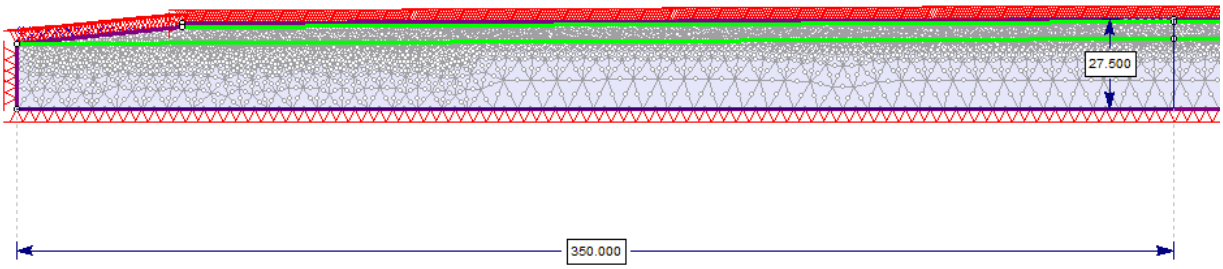

Figure 5.3: Left boundary to peak of slope

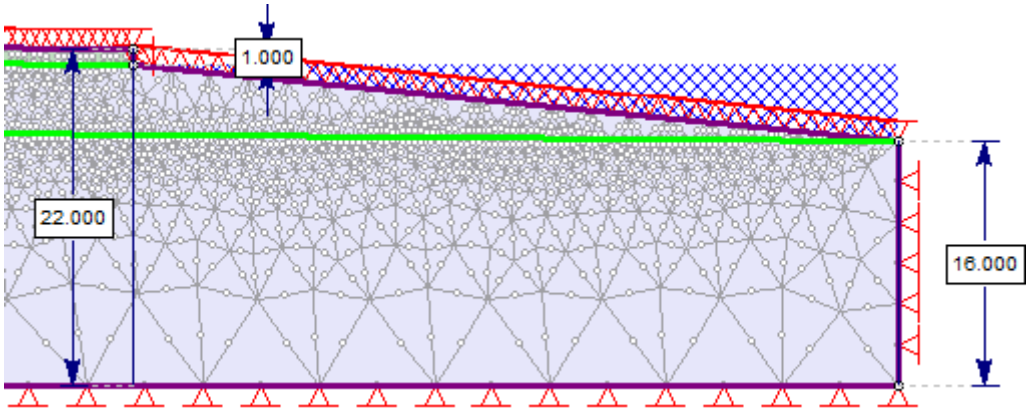

Figure 5.4: Right boundary geometry

5.3. Model Properties

Table 5.1 shows the material properties of the sand and interface material.

Table 5.1: Material properties

Material	Parameter	Value
Sand	Porosity	0.1
	Hydraulic properties	
	Model	User defined
	Behaviour	Drained
	K2/K1	0.01
	K1 Angle (Degrees)	0
	Mv (m3/m3)	1e-10

	User permeability and WC	Defined
	Thermal properties	
	Water content (m3/m3)	0.1
	Unfrozen conductivity (W/m/C)	3.21
	Frozen conductivity (W/m/C)	3.36
	Thermal heat capacity method	Jame Newman
	Latent heat	Yes
	Soil specific heat capacity (J/tons/C)	840000
	Thermal soil unfrozen water content method	Custom
	Thermal expansion	No
	Dispersivity	Yes
	Longitudinal dispersity (m)	5
	Transverse dispersivity (m)	1
Interface	Hydraulic properties	
	Model	Constant
	Behavior	Drained
	Ks (m/s)	1e-20
	K2/K1	1
	K1 angle	0
	WC curve slope	0.4
	Use mv	Yes
	Mv	1e-10
	Thermal properties	
	Unfrozen and frozen conductivity (W/m/C)	1.25
	Thermal heat capacity method	constant
	Latent heat	No
	Frozen and unfrozen het capacity	0
	Thermal soil unfrozen water content	Simple
	Thermal expansion	No
	Dispersivity	No

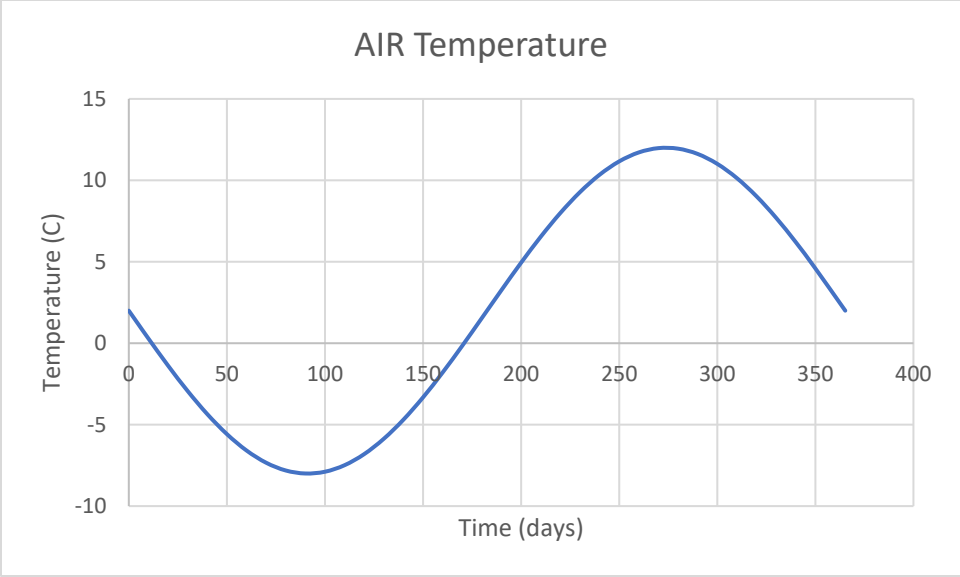

Figure 5.5: Air temperature function

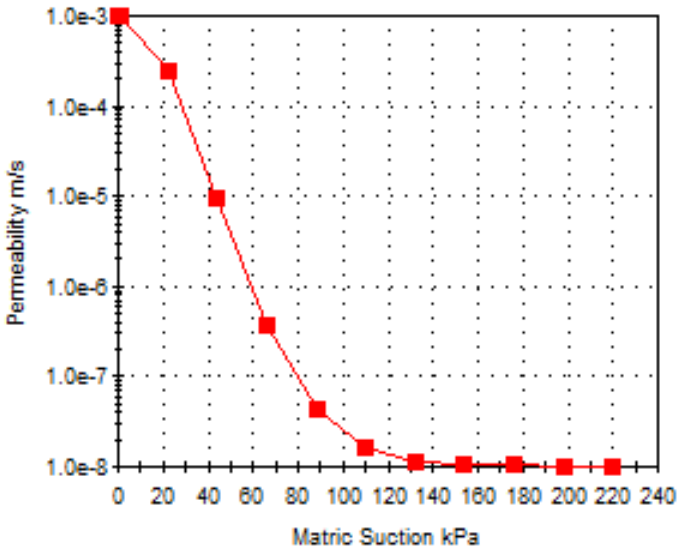

Figure 5.6: Permeability function

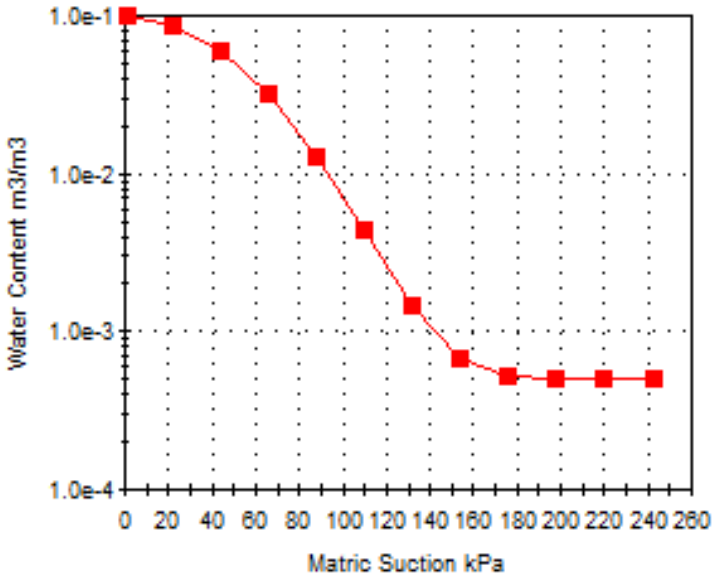

Figure 5.7: Water content function

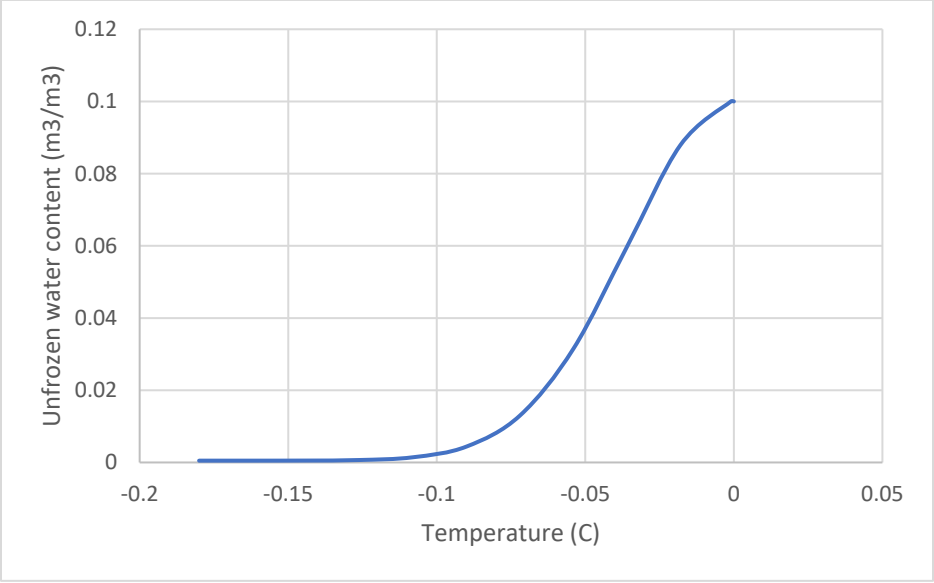

Figure 5.8: Unfrozen water content function

5.4. Results

Seasonal water flow results are shown in Figure 5.9. The results are generally similar to what observed in McKenzie et al. (2007). As in the summertime when the water is allowed to penetrate from the hill top, the water flows from the hill top to the two lakes. In the winter as in the surface ground frozen, the water flows from the lake at higher elevation (on the left) to the lake that has a lower elevation (on the right). User can refer to the example model to see the development of unfrozen water content and its effects on water flow.

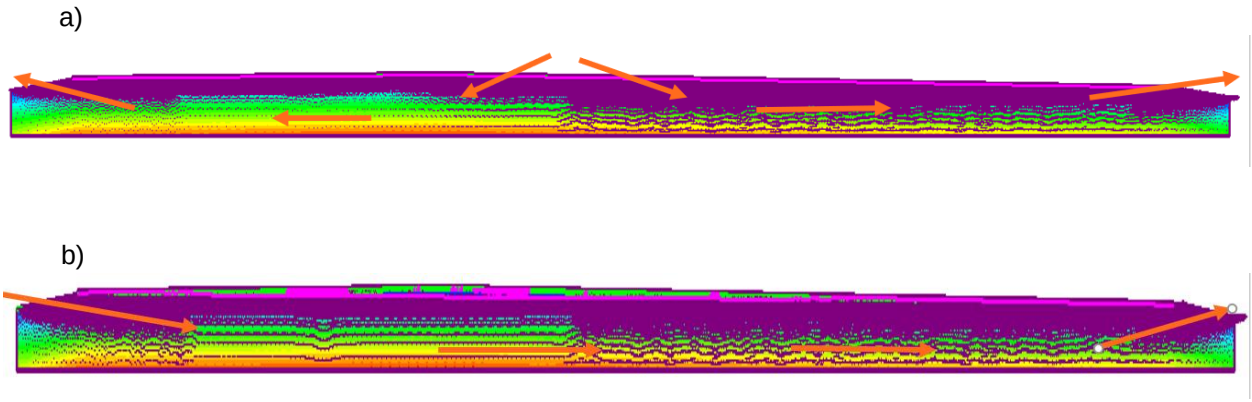

Figure 5.9: Seasonal water flow a) Summer b) Winter

5.5. Reference

McKenzie, J., Voss, C., & Siegel, D. (2007). Groundwater flow with energy transport and water–ice phase change: Numerical simulations, benchmarks, and application to freezing in peat bogs. *Advances In Water Resources, 30(4), 966-983. doi: 10.1016/j.advwatres.2006.08.008.*

6. Geological Repository for Used Nuclear Fuel

6.1. Problem Description

The Nuclear Waste Management Organization (NWMO) have developed plans for the long-term management of used nuclear fuel. This includes the containment and isolation of used fuel in a deep geological repository. In this problem, the feasibility of a two leveled repository and placement of used fuel containers (UFC) will be evaluated by coupled thermo-mechanical modelling of RS2 and compared with the results presented by Carvalho and Zivković, (2018). Long term thermal dissipation and rock damage results will be compared.

6.2. Model Geometry

The model domain comprises of a 2 500m long column with a width of 12.5 m. The top surface of the model is kept at 5˚C and the bottom is kept at 35˚C. There is a vertical temperature gradient of 0.012˚C/m.

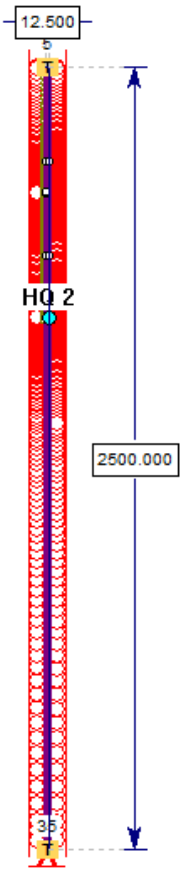

Figure 6.1: RS2 model Geometry

The first repository is excavated and placed at 800m depth and the second at 400m depth. Each repository has two containers which are placed simultaneously in a buffer box. The buffer box consists of 100% bentonite. The remaining spaces between the UFC and the walls of the excavated placement area

is filled with bentonite pellets (gap fill) and compacted bentonite. The geometry of the repository is seen in figure 2.

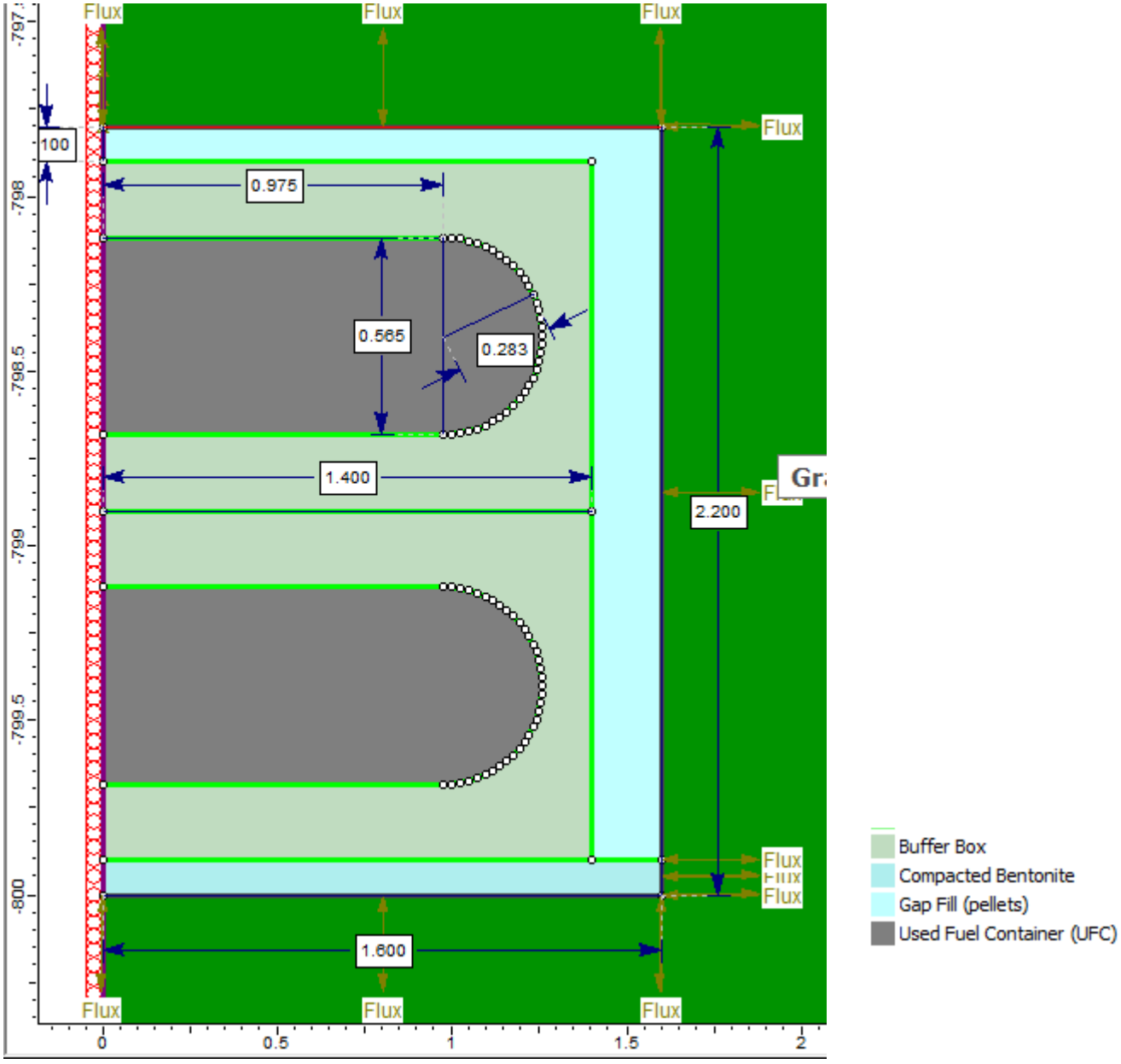

Figure 6.2: Repository geometry

Heat is generated by the containers once they are placed in the repository. Each container is 30 years out of reactor before they are placed in their respective repository and therefore generate a heat of 169 W (Carvalho and Zivković, 2018). A time dependant flux (Table 6.1) was applied along the sides of the repository to simulate the heat generation.

Table 6.1: Heat flux function

Time (years)	Heat flux (W/m^2)
0	20.8642
10	17.5309
20	15.0617
30	12.963
45	10.6049
70	8.06173
120	5.69136
170	4.77778
270	4.04938
469.9994	3.30864
969.9994	2.2963
9970.003	0.81358
99969.88	0.0469136
999971.5	0.017284
9999968	0.0111111

The second repository (at 400m) was excavated and placed 20 years after the first was installed. The analysis is taken over a total of 1000 years to observe the long-term effects of the heat generation.

6.3. Model Properties

The crystalline rock which surrounds each repository is a granitic gneiss. The mechanical and thermal properties of the rock mass and engineered materials used is found in Table 6.2, Table 6.3 and Table 6.4.

Table 6.2: Material properties

Material	Initial element loading	Unit weight (MN/m^3)	Poisson's ratio	Young's modulus (J/m^3/C)	residual young's modulus	Unloading conditions
Granitic Gneiss	Field stress and Body force	0.0265	0.5	45 000	no	no

Buffer box	Body force only	0.0167	0.5	150	no	no
Compacted Bentonite	Body force only	0.0157	0.5	100	no	no
Gap fill (pellets)	Body force only	0.0138	0.5	100	no	no
Used Fuel container (UFC)	Body force only	0.054	0.5	200 000	no	no

Table 6.3: Strength parameters

Material	Parameter	Value
Granitic Gneiss	Failure criterion	Generalized Hoek-Brown
	Material type	Plastic
	Compressive strength (MPa)	210
	mb	16.5
	s	0.1
	a	0.501
	Residual mb	16.5
	Residual s	0.1
	Residual a	0.501
	Dilation	0
	Tensile cutoff type	None
Buffer box	Failure criterion	Mohr-Coulomb
	Material type	Elastic
	Peak tensile strength (MPa)	0.022
	Peak friction Angle (degrees)	30
	Peak Cohesion (MPa)	0.217
Compacted Bentonite	Failure criterion	Mohr-Coulomb
	Material type	Elastic
	Peak tensile strength (MPa)	0.022
	Peak friction Angle (degrees)	30

	Peak Cohesion (MPa)	0.217
	Failure criterion	Mohr-Coulomb
Gap fill (pellets)	Failure criterion	Mohr-Coulomb
	Material type	Elastic
	Peak tensile strength (MPa)	0.022
	Peak friction Angle (degrees)	30
	Peak Cohesion (MPa)	0.217
Used Fuel container (UFC)	Material type	Elastic

Table 6.4: Thermal properties

Material	Conductivity (W/m/C)	Heat capacity (J/m^3/C)	Latent heat	Thermal expansion	Dispersivity
Granitic Gneiss	3	2.2815e+06	no	1e-05	no
Buffer box	1	2.176e+06	no	no	no
Compacted Bentonite	0.45	1.36e+06	no	no	no
Gap fill (pellets)	0.4	1.2267e+06	no	no	no
Used Fuel container (UFC)	1e-06	1e-06	no	no	no

6.4. Results

A history query (HQ1) is placed aligned with the midpoint of the lower repository along the far side of the rock column. Another query (HQ2) is placed aligned with the midpoint of the lower repository along the side wall. The temperature history at these points is compared between RS2 and Carvalho and Zivković (ARMA, 2018) (Figure 6.3).

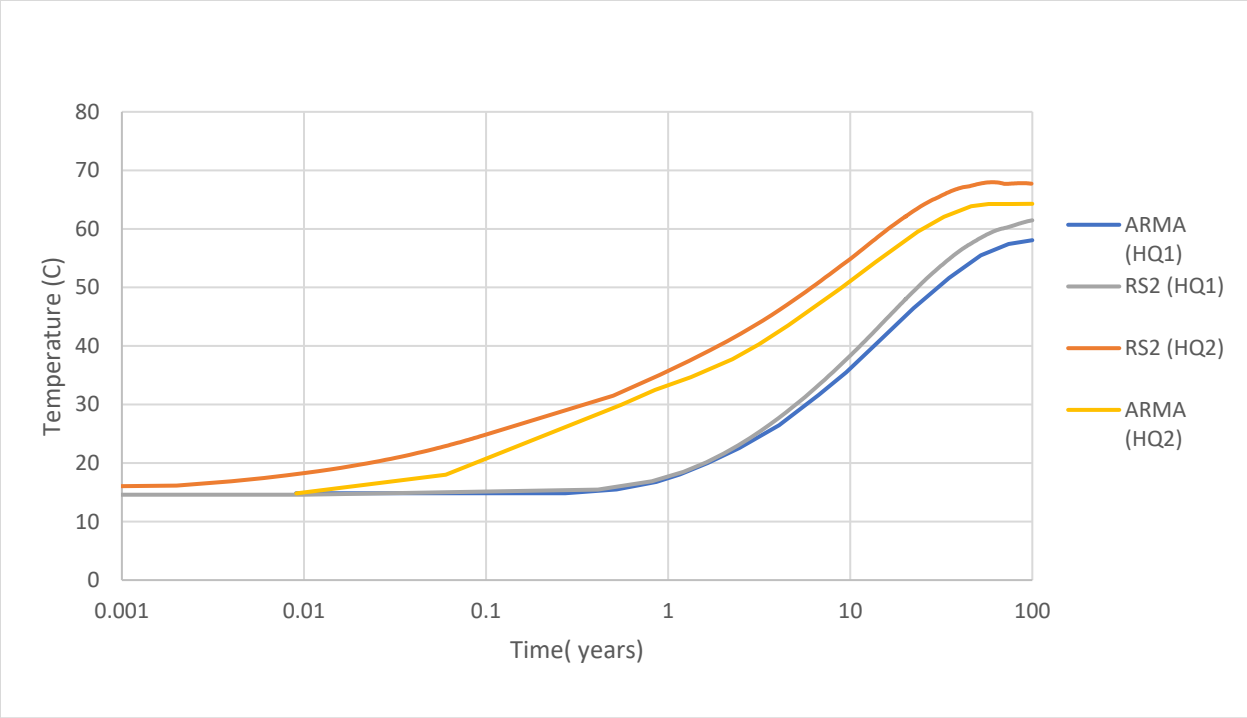

Figure 6.3: Temperature history at history query

Figure 6.4 and Figure 6.5 shows damage incurred immediately after excavation and 1000 years after. Carvalho and Zivković (2018) reports the damage after excavation is limited to 0.1m or less around the area. The heat produced by the containers induce thermal stresses and damage extends to 0.4m on the roof and 0.2 on the side after 1000 years. At the last stage, the model does not converge because of the excessive failure due to the thermal expansion. Differences can be due to the residual values of the material strength not being accounted for in the RS2 model.

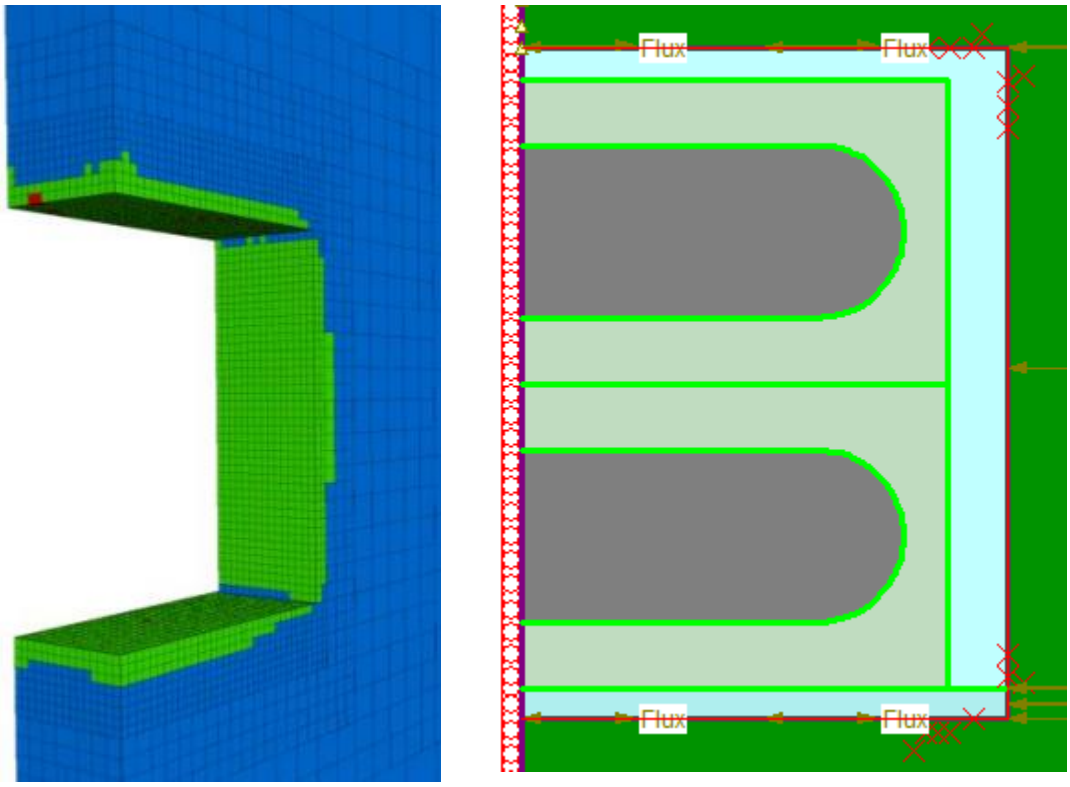

Figure 6.4: Yield elements after excavation

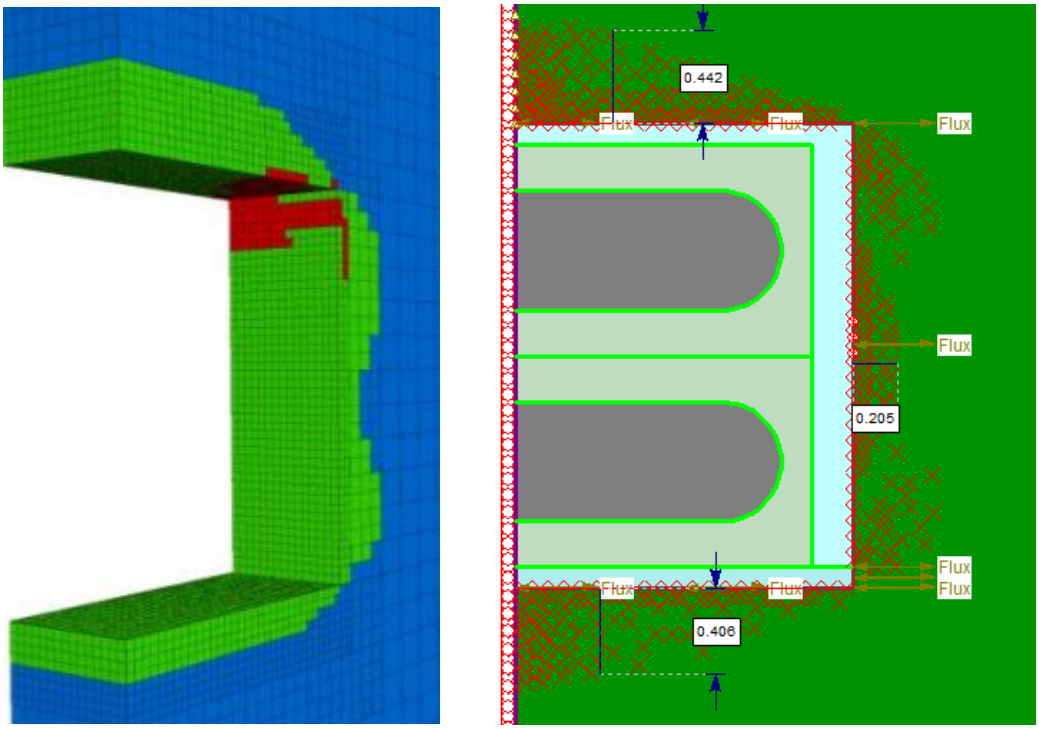

Figure 6.5: Yield elements time = 1000 years

6.5. References

Carvalho, J. and Zivković, A. (2018). Near-field and far-field thermal-mechanical modelling of a two-level deep geological repository for used nuclear fuel in crystalline rock – an update. *ARMA*, 18(1373).

7. Heat Loss from Basement

7.1. Problem Description

This problem addresses the use of RS2 to simulate heat transfer from a basement foundation. Two scenarios are considered: model 1) uninsulated concrete walls; and model 2) insulated concrete walls; insulation on the interior wall face.

7.2. Model Geometry

The basement is 3m long and 2m wide as seen in Figure 7.1. The analysis takes place over a period of 100 days. The initial temperature of the top boundary and basement is set to 6.97˚C and the bottom boundary set to 3.97 ˚C. At the second stage, the basement concrete is implemented, and the top surface is subjected to a time dependent flux of climatic conditions and the basement exterior walls is set to 20˚C, as seen in Figure 7.2. Similarly with the insulated model, insulation and concrete material is implemented in stage 2, seen in Figure 7.3.

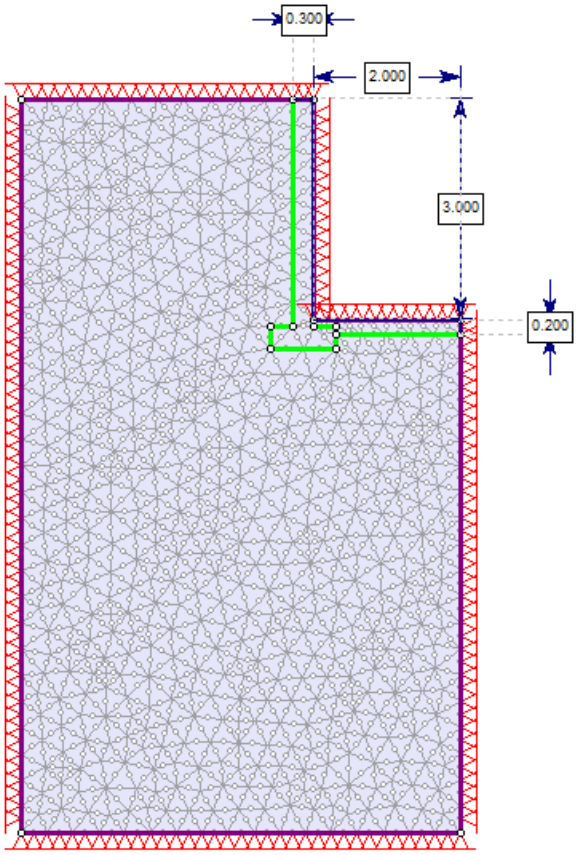

Figure 7.1: Geometry of RS2 models

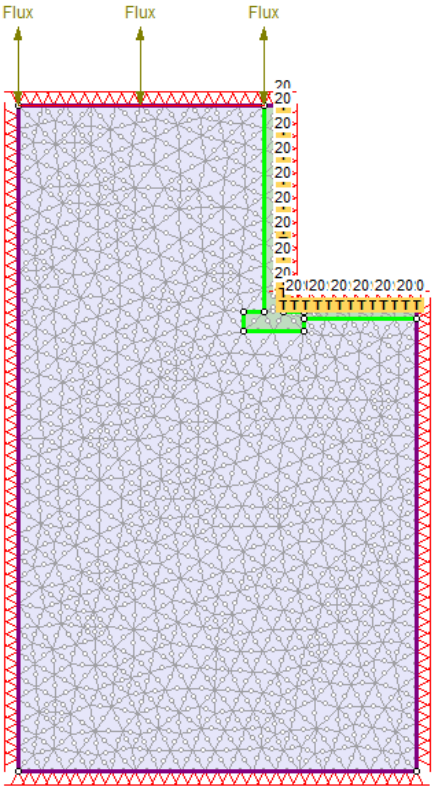

Figure 7.2: RS2 model 1 second stage

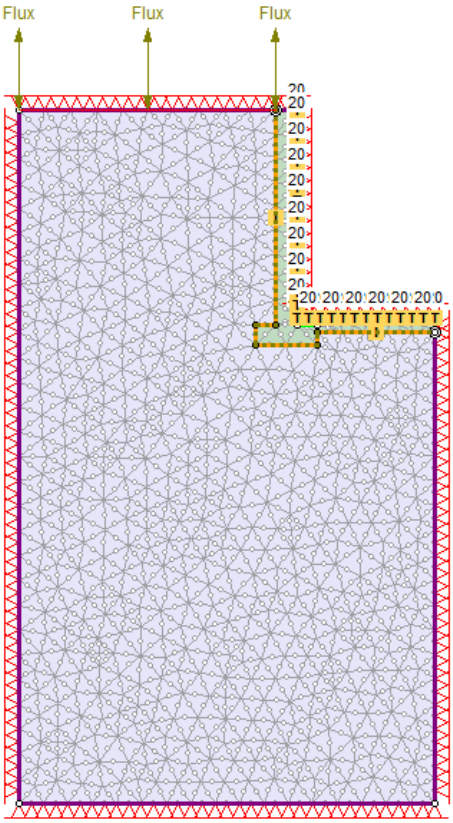

Figure 7.3: RS2 model 2 second stage

7.3. Material Properties

The material properties of the soil, concrete and insulation used in the model can be found in Table 7.1.

Table 7.1: Model properties

Material name	Parameters	Value
Clay	**Hydraulic properties**	
	Material behaviour	Drained
	Static water mode	dry
	Thermal Properties	
	Water content value	0.5
	Thermal Conductivity Method	Johansen
	Soil type	Fine
	Quartz content	0.74
	Thermal volumetric heat capacity type	Jame Newman
	Include latent heat	Yes
	Thermal soil unfrozen water content type	Simple
Concrete	**Hydraulic properties**	
	Material behaviour	Drained
	Static water mode	dry
	Thermal Properties	
	Water content value	0.1
	Thermal Conductivity Method	Constant
	Unfrozen conductivity (KJ/s/m/˚C)	0.0015
	Frozen conductivity (KJ/s/m/˚C)	0.0015
	Thermal volumetric heat capacity type	Constant
	Include latent heat	No
	Unfrozen and frozen heat capacity ($KJ/m^3/˚C$)	2000
	Thermal soil unfrozen water content type	Simple
Insulator	Thermal conductivity (KJ/s/m/˚C)	0.000004

The inputs for the climate conditions are as follows:

Table 7.2: Top boundary flux climate conditions

Type	Data
Start time	0 s
Total time	427 days
Radiation	Calculate from Solar Radiation
Define Vegetation	yes
Define snow pack	yes
Snow conductivity	0.0001

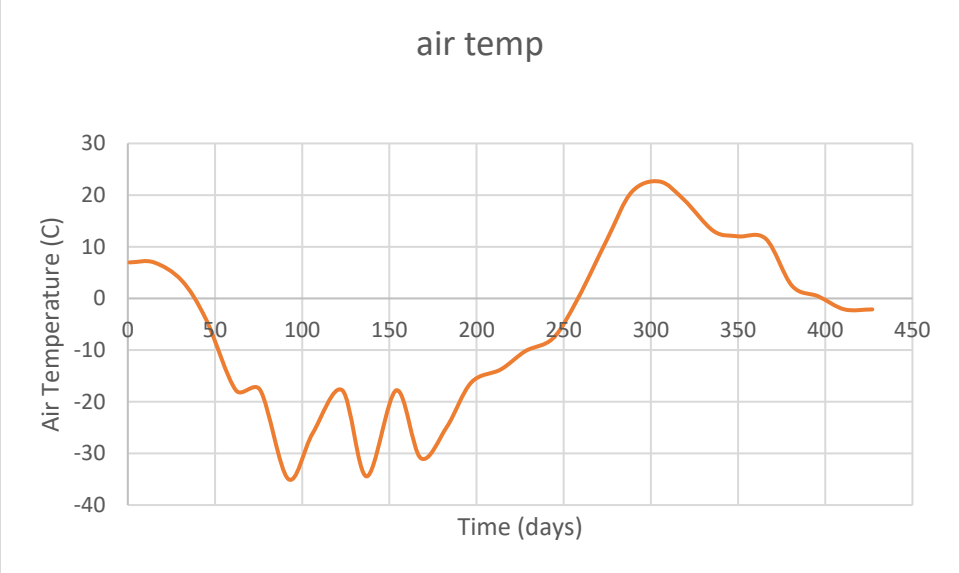

Figure 7.4: Air temperature vs. time

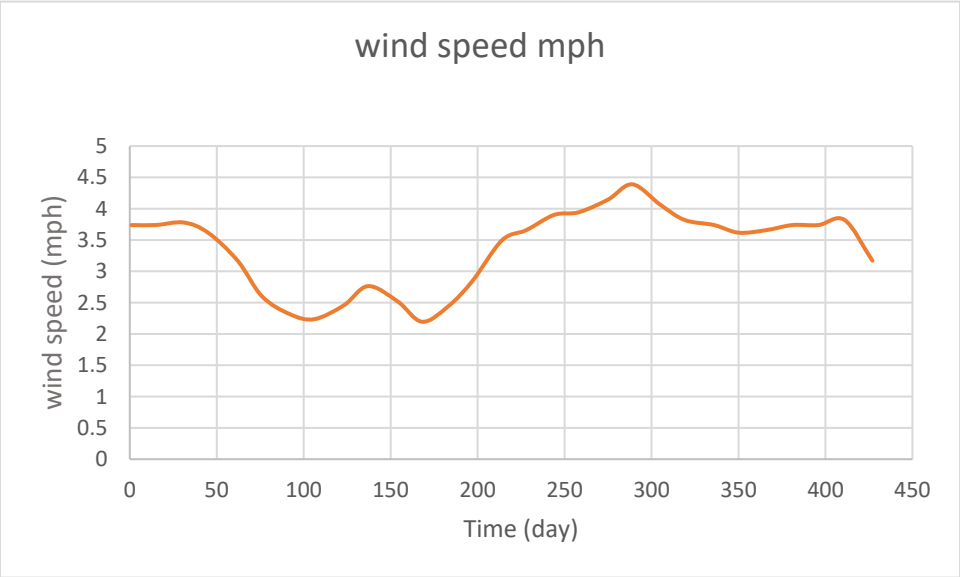

Figure 7.5: Wind speed vs. time

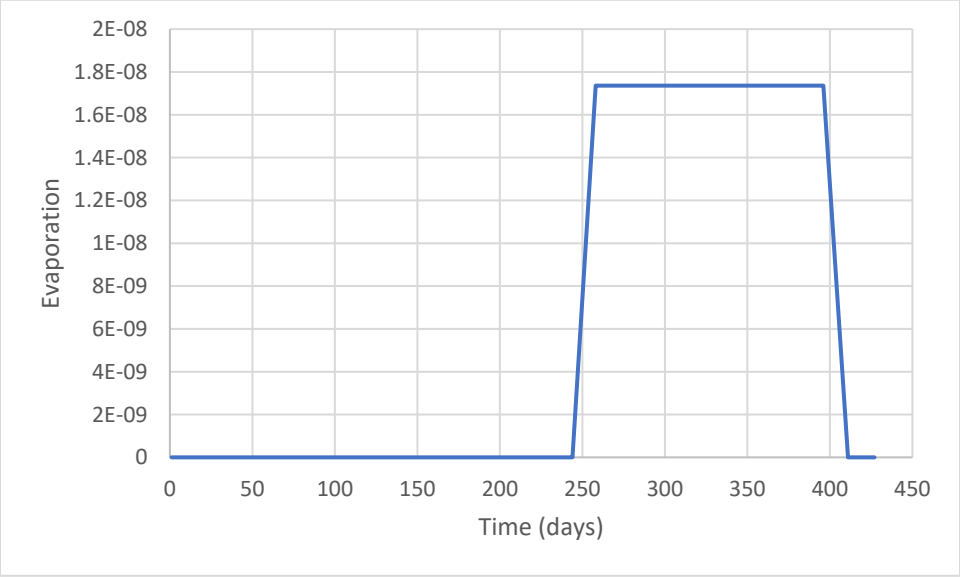

Figure 7.6: Evaporation vs. time

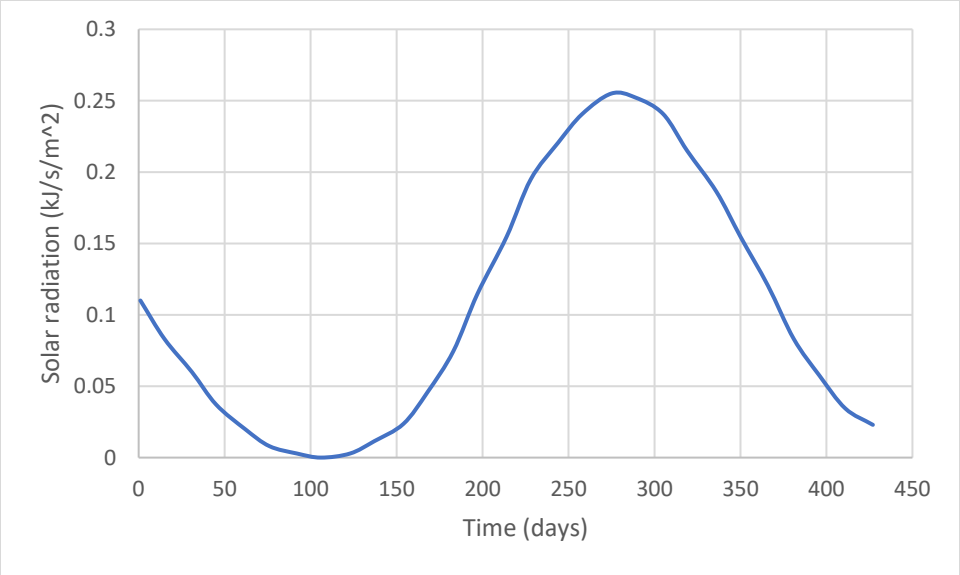

Figure 7.7: Solar radiation vs. time

7.4. Results

The temperature contour seen in Figure 7.8 illustrates the influence of the uninsulated basement on the surrounding soil. As shown, the temperature at the reference point 2m below the ground surface and 1 m left of the basement wall is 11.03˚C on day 100. The contours are changed significantly in the presence of insulation, as seen in Figure 7.9. The insulation provides a substantial barrier to heat loss and thus the temperature at the reference point is much lower, 3.39 ˚C.

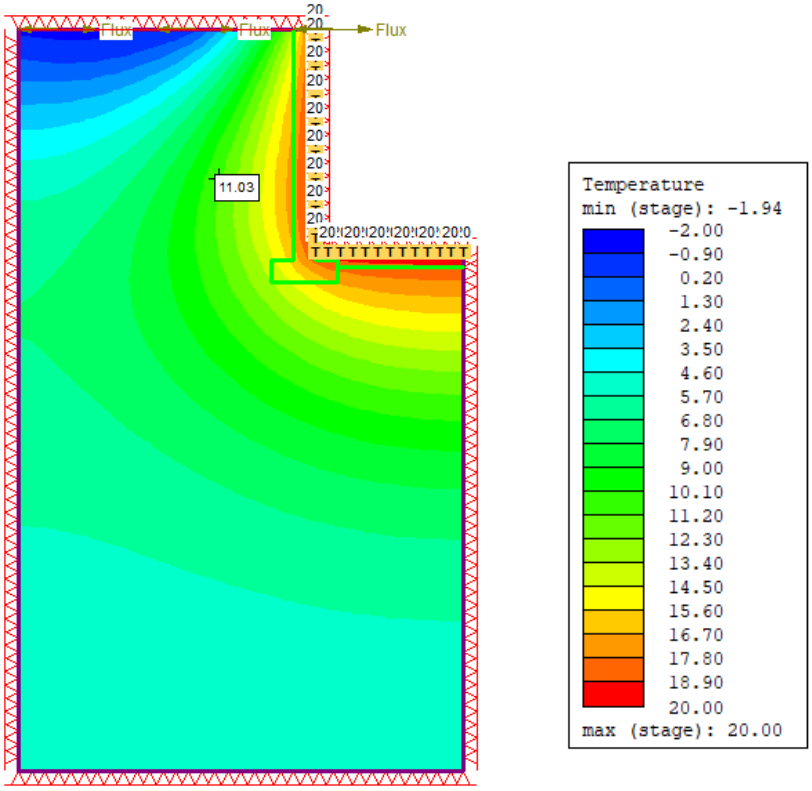

Figure 7.9: Temperature contour on day 100 for the uninsulated basement

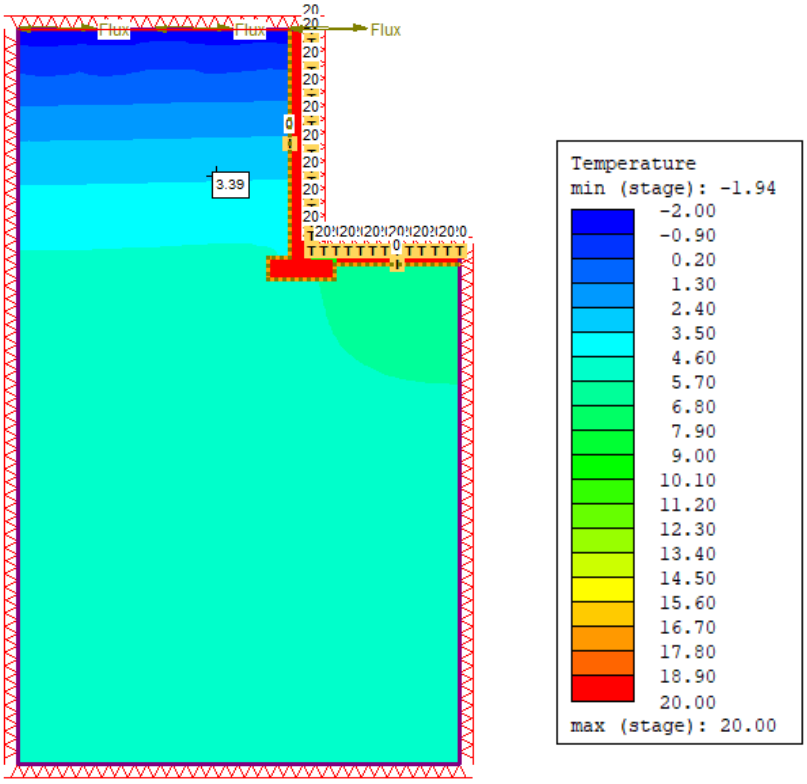

Figure 7.8: Temperature contour on day 100 for the insulated basement

The rate of heat loss (heat rate) across the face of the vertical basement wall in both the insulated and non insulated model is greatest at the beginning of the analysis and proceeds to a steady state.

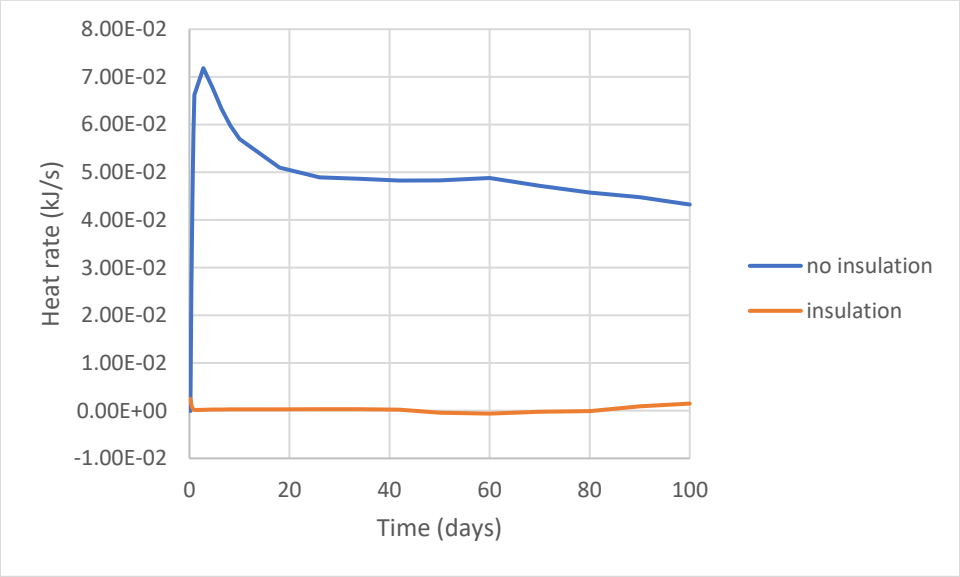

Figure 7.10: Heat rate function across vertical wall

8. Effects of Climates on Slope Stability

8.1. Problem Description

This problem addresses the use of RS2 to simulate the effects of climate on slope stability. An embankment underlain by a foundation is modelled. There are four models in the example. First one is the mode that has no geosynthetic. Second one has geosynthetic installed to increase the SRF from 1.15 to 1.25. Third one has flux climate boundary condition applied with geosynthetic. Fourth one monitors the climate effect over time. Comparing the results for all four models, the impact of climate effect on slope stability can be observed.

8.2. Model Geometry

All four models share the same geometry. The model comprises of a foundation layered by five types of clay. The foundation is 24m in height and 90m in width. The sloped embankment on top of the foundation consists of four materials, with a 1 m-thick first layer. The embankment is 5m height and 50m width in total, with slopes on both sides. The coordinates of the embankment are (0,0), (-8.610,7), (-31.915, 7), (-35.605, 4), (-50, 4), and (-50, 0).

Model 1

No geosynthetic, no climate effects.

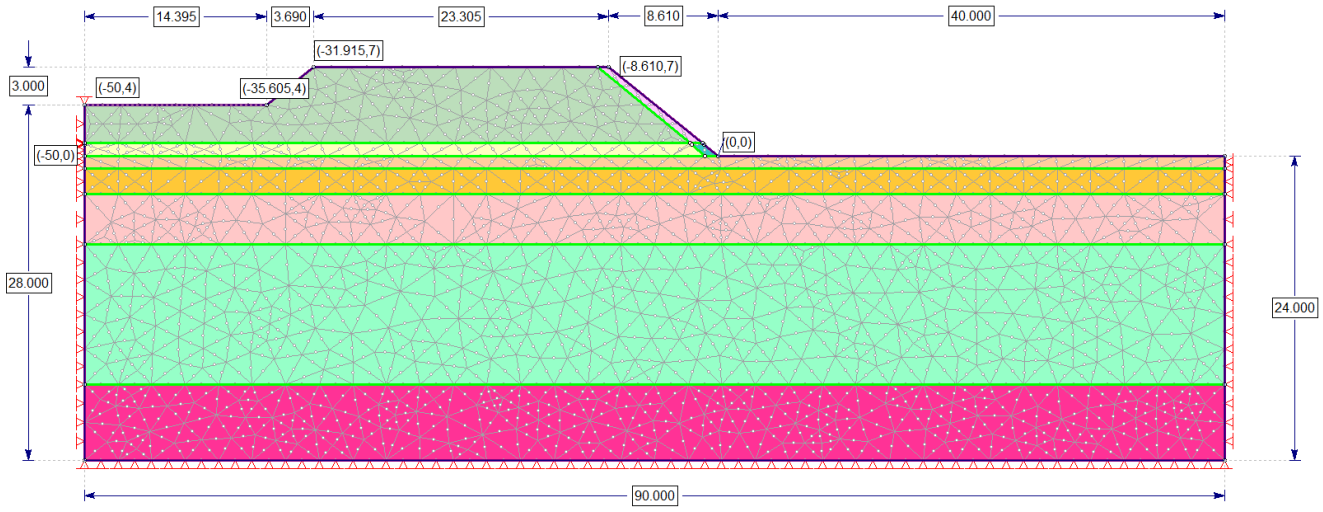

Figure 8.1: Model 1 geometry

Model 2

A geosynthetic with joints as slip on both sides is added as a structural interface in RS2. The geosynthetic is applied to the top of lower embankment layer. Note that the thermal effect on geosynthetic including the thermal expansion is considered in this model (see Table 8.6 below). No climate effects.

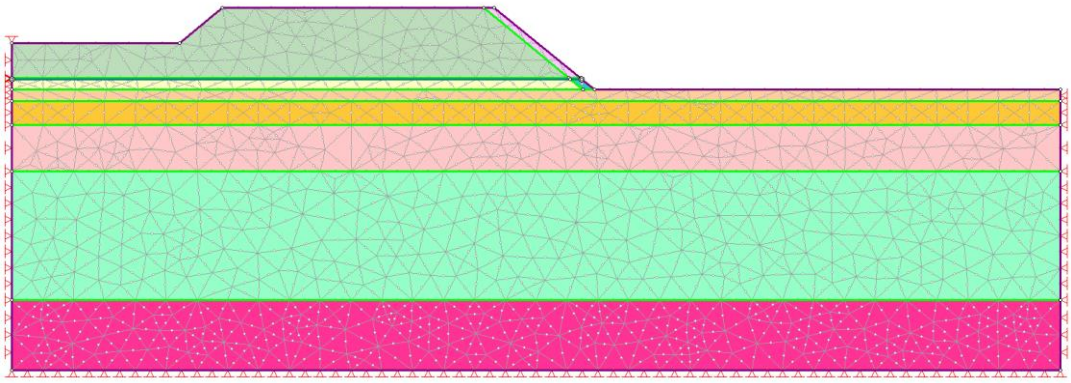

Figure 8.2: Model 2 geometry

Model 3

A geosynthetic is included the same way as in model 2. Thermal boundary conditions are applied to account for the climate effect on slope stability. The analysis is taken over 182.5 days, which initially started in August. The stages are set at day 0 and day 182.5 (February). An initial temperature of 1 °C is assigned to the domain. An initial temperature of 2 °C is applied to all sides of boundaries except for the bottom boundary. In February, a constant heat flux of 8e-05 kJ/d/m is applied to the bottom boundary, and a time dependent flux climate boundary condition is applied along the top boundary. The data for flux climate condition on the top boundary are shown in Table 8.1 and Table 8.2, and from Figure 8.4 to Figure 8.9 later in the section.

Model 4

A geosynthetic is included the same way as in model 2. Thermal boundary conditions included the same ways as in model 3. An additional stage at day 319 (June) is added to observe the climate effect with respect to the time.

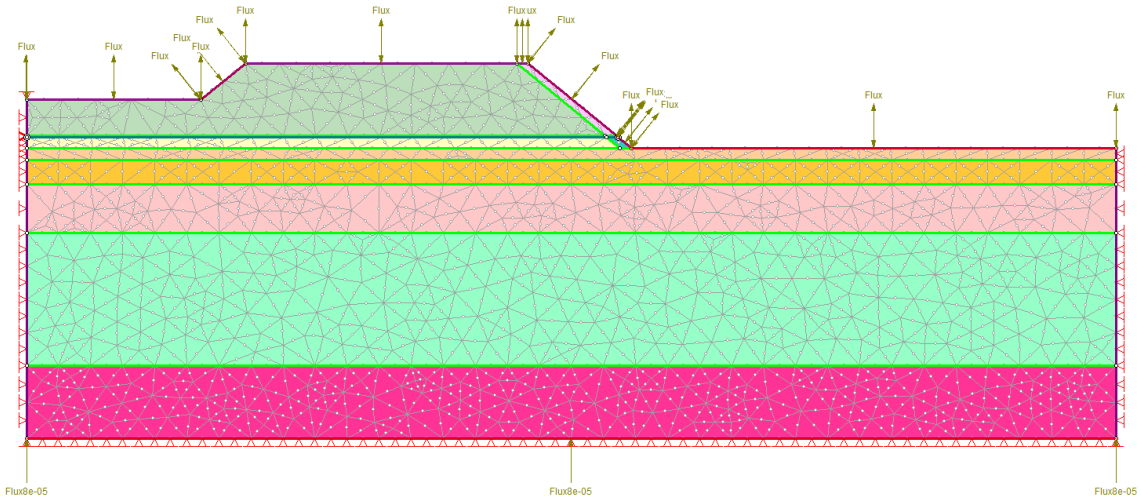

Figure 8.3: Model 3 and 4 geometry

The top boundary flux climate condition inputs are shown in Table 8.1 and Table 8.2, and Figure 8.4 to Figure 8.9 below.

Table 8.1: Top boundary flux climate conditions

Type	Data
Start time	0 s
Total time	1e+10 days
Radiation	Calculate from Solar Radiation
Define vegetation	yes
Define snow pack	yes
Snow conductivity (kW/m/C)	0.0001

Table 8.2: Vegetation height time function

Time (d)	Vegetation height (m)
0	0.001
1e+09	0.001

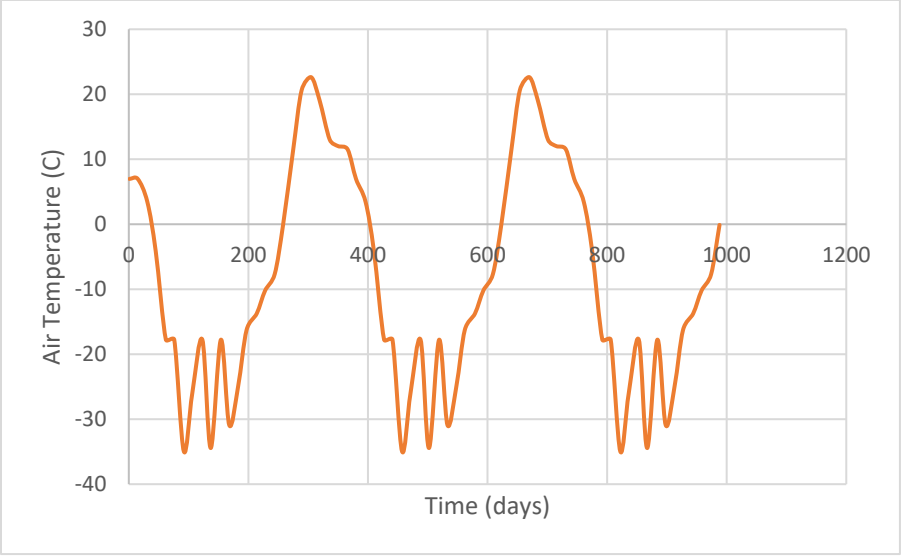

Figure 8.4: Air temperature vs. time

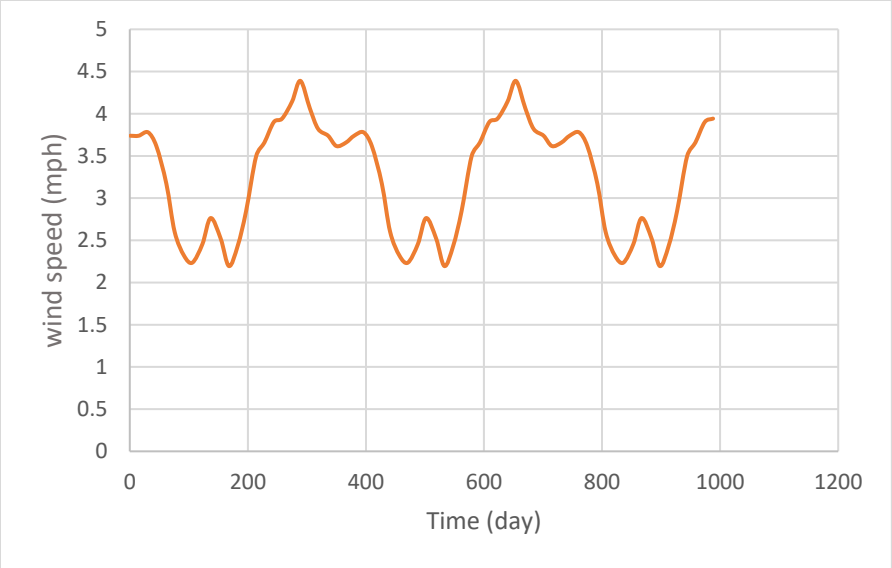

Figure 8.5: Wind speed vs. time

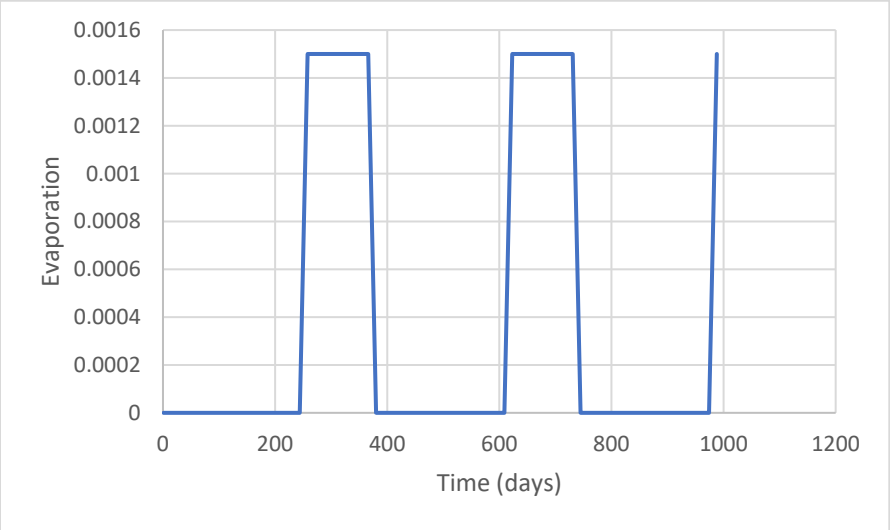

Figure 8.6: Evaporation vs. time

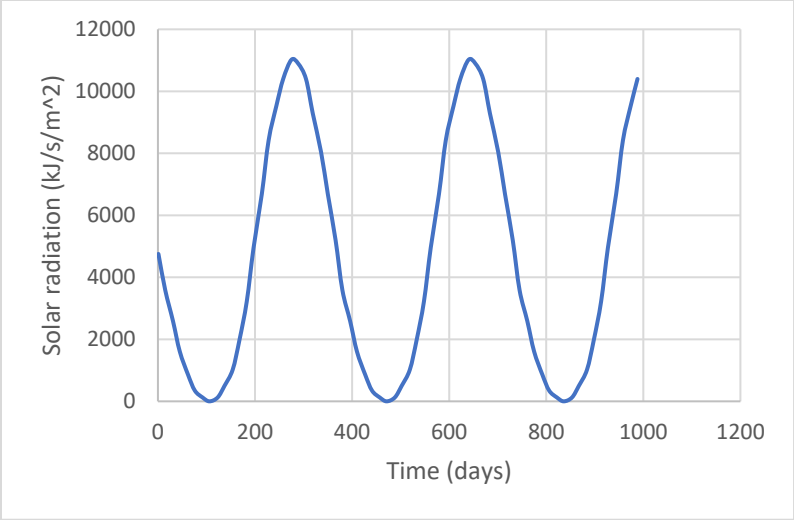

Figure 8.7: Solar radiation vs. time

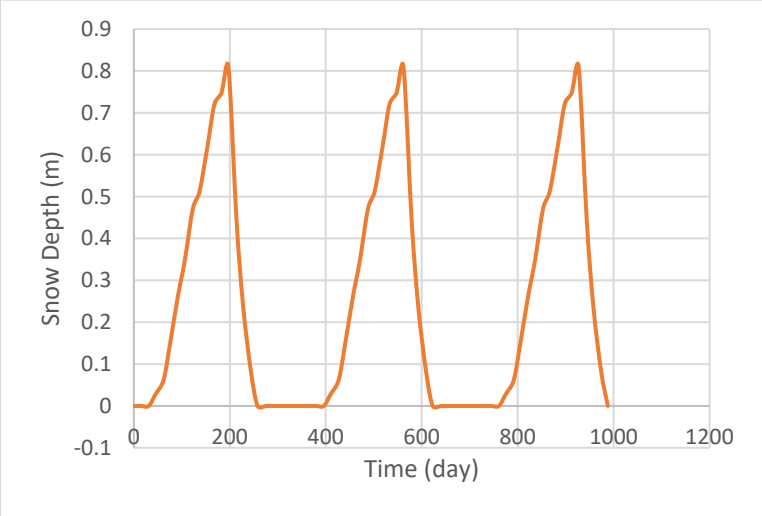

Figure 8.8: Snow depth vs. time

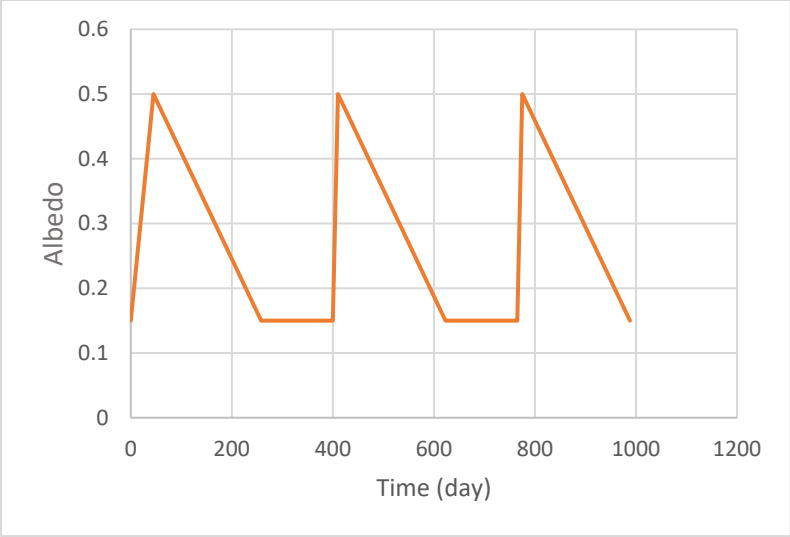

Figure 8.9: Albedo vs. time

8.3. Material Properties

The material properties are shown in Table 8.3 to Table 8.5 below.

Table 8.3: Mechanical properties

		Embankment upper	Embankment upper elastic	Embankment lower	Embankment lower elastic	Clay 1	Clay 2	Clay 3	Clay 4	Clay 5
Initial element loading		Field stress and body force								
Unit weight (kN/m3)		21.9	21.9	17.2	17.2	18	17.5	13.5	17	17.5
Porosity value		0.5	0.5	0.5	0.5	0.5	0.5	0.5	0.5	0.5
Poisson's ratio		0.4	0.4	0.4	0.4	0.4	0.4	0.4	0.4	0.4
Young's Modulus (kPa)		50 000	50 000	50 000	50 000	50 000	50 000	50 000	50 000	50 000
Failure criterion		Mohr-Coulomb								
Material type		Plastic	Elastic	Plastic	Elastic	Plastic	Plastic	Plastic	Plastic	Plastic
Peak strength	Peak tensile strength (kPa)	0	0	0	0	43	31	30	32	32
	Peak friction angle (degrees)	35	35	33	33	0	0	0	0	0
	Peak cohesion	0	0	0	0	43	31	30	32	32

Residual strength	Residual friction angle (degrees)	35	N/A	33	N/A	0	0	0	0	0
	Residual cohesion (kPa)	0	N/A	0	N/A	43	31	30	32	32
	Dilation angle (degrees)	0	N/A	0	N/A	0	0	0	0	0
	Apply SSR	Yes	N/A	Yes	N/A	Yes	Yes	Yes	Yes	Yes

Table 8.4: Hydraulic properties

Material name	Material behaviour	Static water mode	Ru value
Embankment upper	Drained	Ru	0
Embankment upper elastic			
Embankment lower			
Embankment lower elastic			
Clay 1			
Clay 2			
Clay 3			
Clay 4			
Clay 5			

Table 8.5: Thermal properties

Material name	Water content	Thermal Conductivity	Soil type	Quartz content	Thermal heat capacity	Include latent heat	Soil specific heat capacity (kJ/ton/C)	Thermal soil unfrozen water content	Thermal expansion	Dispersivity
Embankment upper	Use from Groundwater	Johansen	Fine	0.74	Jame New man	No	500	Simple	No	No

Embankment upper elastic	Use from Groundwater	Johansen	Fine	0.74	Jame New man	No	500	Simple	No	No
Embankment lower	Use from Groundwater	Johansen	Fine	0.74	Jame New man	No	755	Simple	No	No
Embankment lower elastic	Use from Groundwater	Johansen	Fine	0.74	Jame New man	No	500	Simple	No	No
Clay 1	Use from Groundwater	Johansen	Fine	0.74	Jame New man	Yes	755	Simple	No	No
Clay 2	Use from Groundwater	Johansen	Fine	0.74	Jame New man	Yes	755	Simple	No	No
Clay 3	Use from Groundwater	Johansen	Fine	0.74	Jame New man	Yes	755	Simple	No	No
Clay 4	Use from Groundwater	Johansen -Lu	Fine	0.74	Jame New man	Yes	755	Simple	No	No
Clay 5	Use from Groundwater	Johansen -Lu	Fine	0.74	Jame New man	Yes	755	Simple	No	No

The geosynthetic properties are given in Table 8.6 below. The liner properties on both sides of the geosynthetic are given in Table 8.7 below.

Table 8.6: Geosynthetic properties

Parameter	Value
Liner type	Geosynthetic
Geosynthetic unit weight (kN/m)	0.05
Initial Temperature (C)	2
Reinforcement type	ACE Geosynthetics – ACEGrid GG30-I
Tensile modulus (kPa)	200,000
Material type	Plastic

Tensile strength (peak) (kN/m)	400
Thermal properties	
Activate thermal	Yes
Conductivity(kW/m/C)	0
Specific heat capacity (kJ/ton/C)	1
Thermal expansion	Yes
Expansion coefficient	0.00017

Table 8.7: Joints properties

Parameter	Value
Slip criterion	Mohr-Coulomb
Peak friction angle (deg)	30.96

8.4. Results

Figure 8.10 to Figure 8.16 show the maximum shear strain contours for each model, and the axial force along the geosynthetic in model 2, 3 and 4. As the climate getting colder in February, the geosynthetic shrink and created more tension along the geosynthetic, it excesses the capacity of 400, the capacity reduced to residual value of 0 at the middle section of geosynthetic, thus the SRF value of the slope reduced to 1. As the weather gets warmer in June, the geosynthetic expand and relax the tension, thus there is less force to keep the slope stable. The SRF further reduced to 1.15 which is the same with the case that we have no reinforcement for the slope.

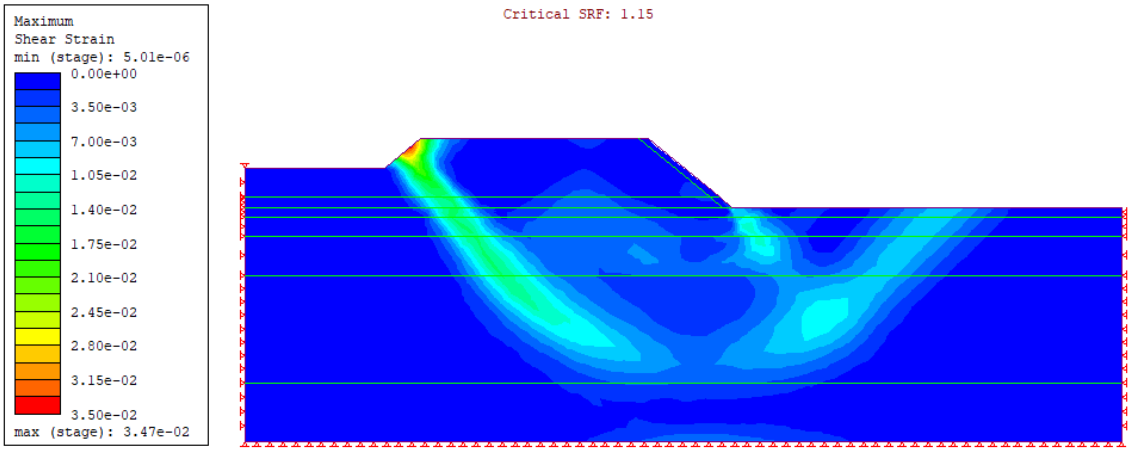

Figure 8.10: Model 1 (no geosynthetic)

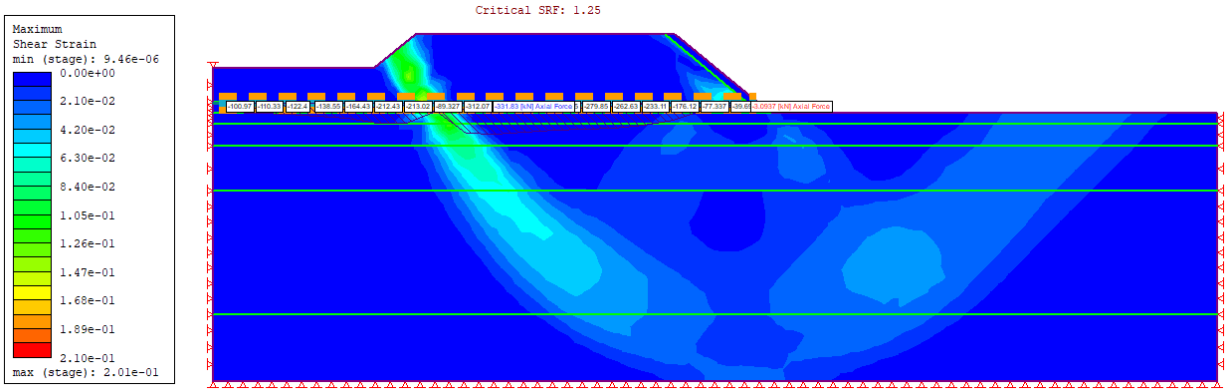

Figure 8.11: Model 2 (no climate)

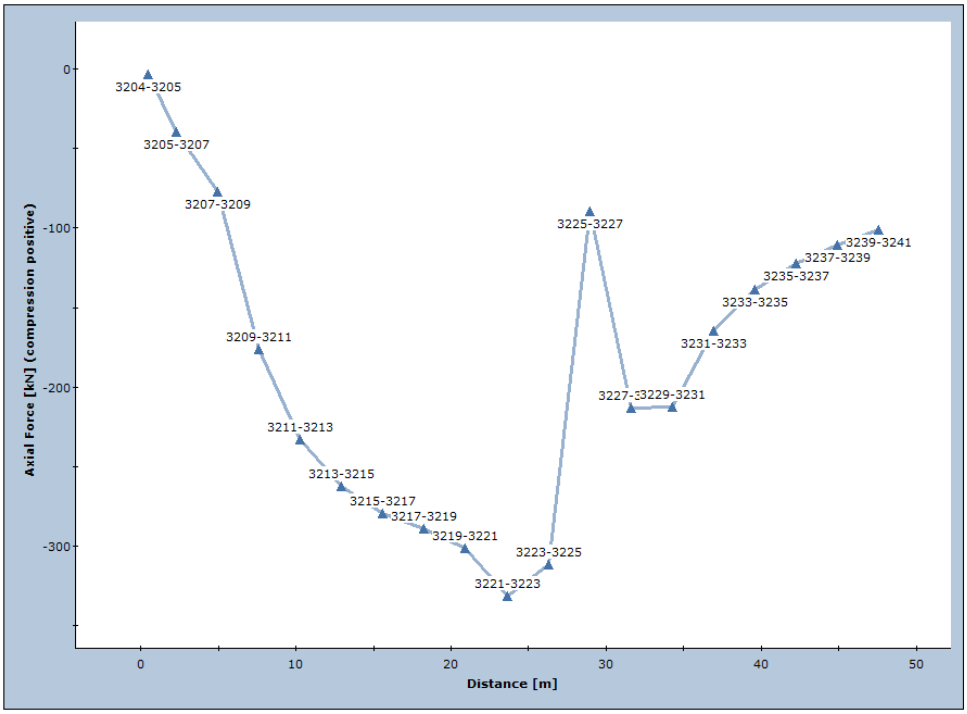

* The numbers beside each point marker represent liner node numbers

Figure 8.12: Model 2 (no climate), axial force along geosynthetic

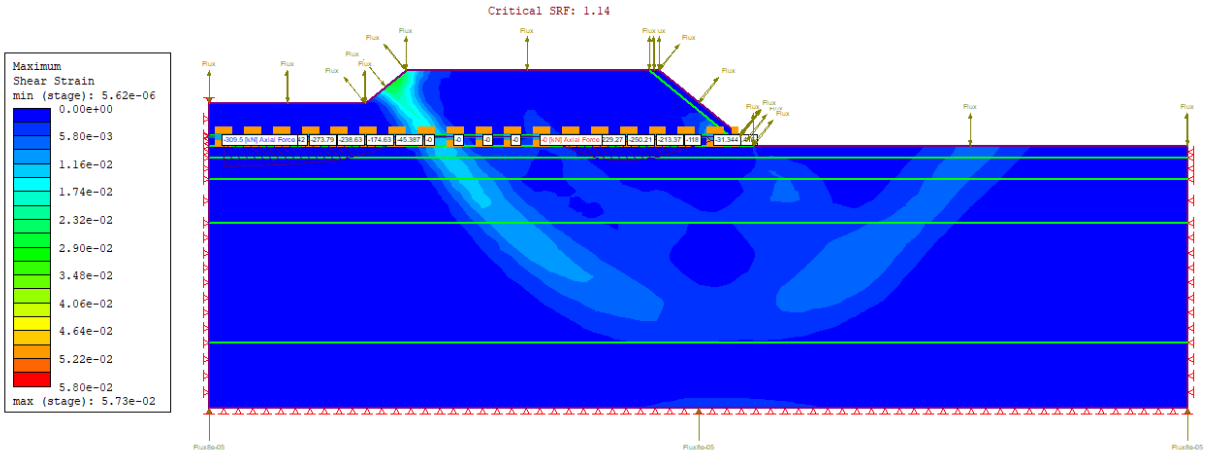

Figure 8.13: Model 3 (Feb)

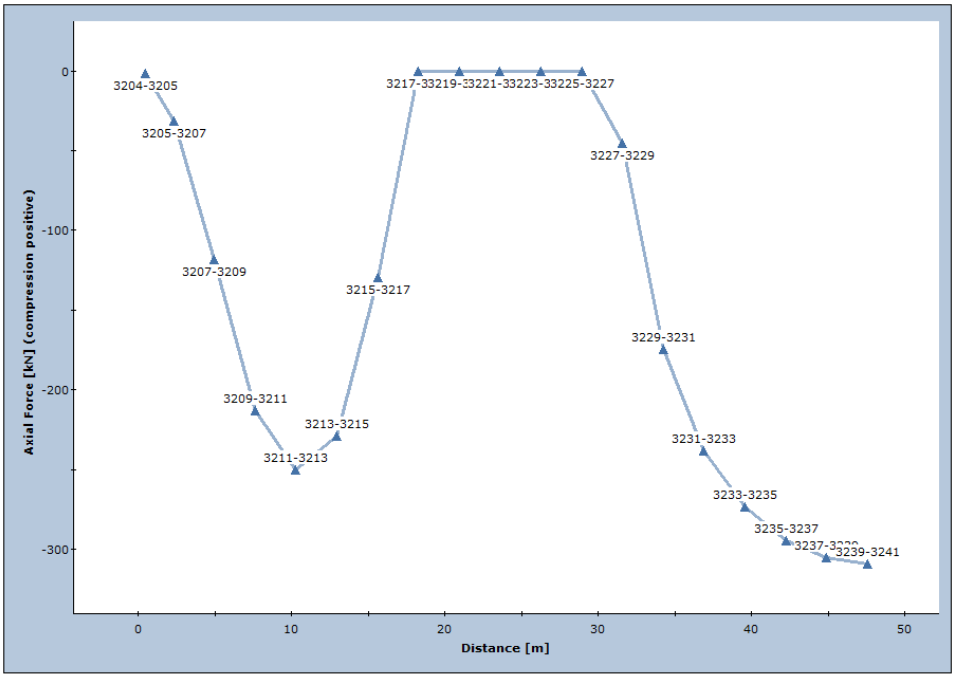

*** The numbers beside each point marker represent liner node numbers**

Figure 8.14: Model 3 (Feb), axial force along geosynthetic

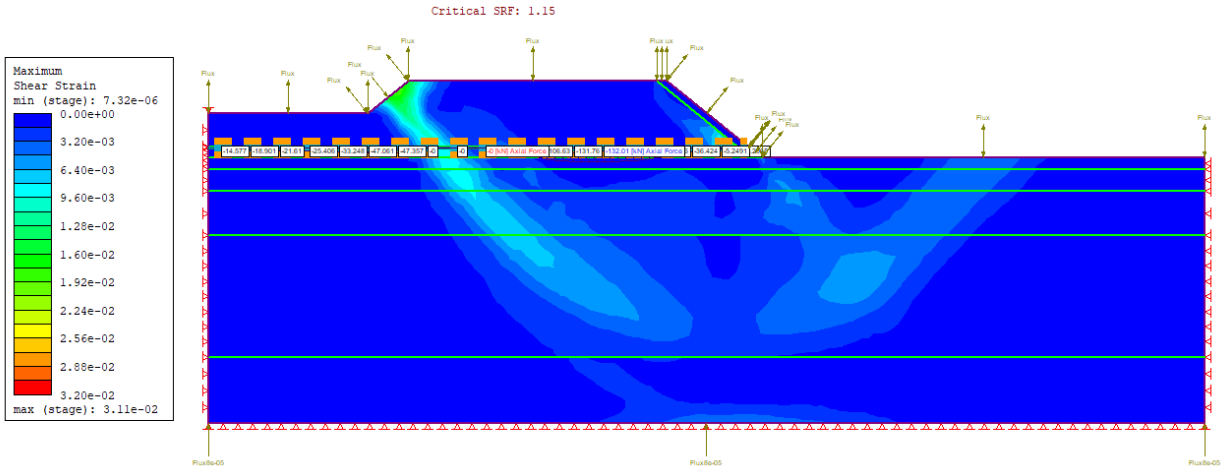

Figure 8.15: Model 4 (June)

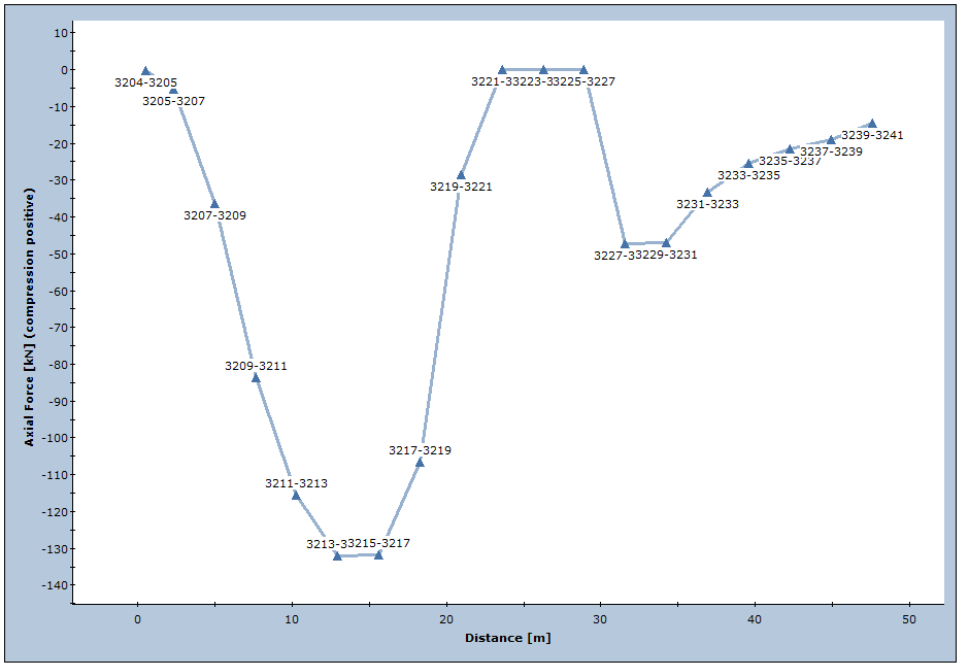

* The numbers beside each point marker represent liner node numbers

Figure 8.16: Model 4 (June), axial force along geosynthetic